bioRxiv preprint doi: https://doi.org/10.1101/2022.02.15.480566; this version posted February 17, 2022. The copyright holder for this preprint (which was not certified by peer review) is the author/funder, who has granted bioRxiv a license to display the preprint in perpetuity. It is made available under aCC-BY-NC-ND 4.0 International license.

1 **Structured and disordered regions of Ataxin-2 contribute differently to the specificity**
2 **and efficiency of mRNP granule formation.**
3

4 Arnas Petrauskas[1*], Daniel L. Fortunati[1*], Amanjot Singh[2], Arvind Reddy Kandi[5], Sai Shruti
5 Pothapragada[2], Khushboo Agrawal[3,4], Joern Huelsmeier[1], Jens Hillebrand[1], Georgia Brown[1],
6 Dhananjay Chaturvedi[2], Jongbo Lee[6], Chunghun Lim[6], Georg Auburger[7], K.
7 VijayRaghavan[2], Mani Ramaswami[1,2†] and Baskar Bakthavachalu[3,5†].

8 *[1]Trinity College Institute of Neuroscience, School of Genetics and Microbiology,*
9 *Smurfit Institute of Genetics and School of Natural Sciences, Trinity College Dublin,*
10 *Dublin-2 Ireland. [2]National Centre for Biological Sciences, TIFR, Bangalore 560065,*
11 *India. [3]Tata Institute for Genetics and Society Centre at inStem, Bellary Road,*
12 *Bangalore 560065, India. [4]School of Biotechnology, Amrita Vishwa Vidyapeetham*
13 *University, Kollam-690525, Kerala, India. [5]School of Basic Sciences, Indian Institute*
14 *of Technology, Mandi 175005, India. [6]Department of Biological Sciences, Ulsan*
15 *National Institute of Science and Technology (UNIST), 50 UNIST-gil, Ulsan 44919,*
16 *Republic of Korea. [7]Experimental Neurology, Medical School, Goethe University,*
17 *60590, Frankfurt, Germany.*

18

19 *These authors contributed equally to this work.
20
21 † **Correspondence**:
22 mani.ramaswami@tcd.ie; Phone +353 (1) 896 8400
23 baskar@iitmandi.ac.in; Phone +91-1905-267705
24
25
26 **Running Title**: Ataxin-2 PAM2:PABP interactions specify granule composition
27
28 **Keywords**: Ataxin-2, TRIBE, mRNA, PABP, Disordered Regions, Subcellular Organization,
29 Stress Granule, Neurodegeneration, RNP Granule, *Drosophila*.
30

bioRxiv preprint doi: https://doi.org/10.1101/2022.02.15.480566; this version posted February 17, 2022. The copyright holder for this preprint (which was not certified by peer review) is the author/funder, who has granted bioRxiv a license to display the preprint in perpetuity. It is made available under aCC-BY-NC-ND 4.0 International license.

31 **ABSTRACT:**

32

33 Ataxin-2 (*ATXN2*) is a gene implicated in spinocerebellar ataxia type II
34 (SCA2), amyotrophic lateral sclerosis (ALS) and Parkinsonism. The encoded protein is a
35 therapeutic target for ALS and related conditions. ATXN2 (or Atx2 in insects) can function in
36 translational activation, translational repression, mRNA stability and in the assembly of
37 mRNP-granules, a process mediated by intrinsically disordered regions (IDRs). Previous work
38 has shown that the LSm (Like-Sm) domain of Atx2, which can help stimulate mRNA
39 translation, antagonizes mRNP-granule assembly. Here we advance these findings through a
40 series of experiments on *Drosophila* and human Ataxin-2 proteins. Results of Targets of RNA-
41 Binding Proteins Identified by Editing (TRIBE), co-localization and immunoprecipitation
42 experiments indicate that a polyA-binding protein (PABP) interacting, PAM2 motif of Ataxin-
43 2 may be a major determinant of the mRNA and protein content of Ataxin-2 mRNP
44 granules. Transgenic experiments in *Drosophila* indicate that while the Atx2-LSm
45 domain may protect against neurodegeneration, structured PAM2- and unstructured IDR-
46 interactions both support Atx2-induced cytotoxicity. Taken together, the data lead to a proposal
47 for how Ataxin-2 interactions are remodelled during translational control and how structured
48 and non-structured interactions contribute differently to the specificity and efficiency of RNP
49 granule condensation as well as to neurodegeneration.

50

51

bioRxiv preprint doi: https://doi.org/10.1101/2022.02.15.480566; this version posted February 17, 2022. The copyright holder for this preprint (which was not certified by peer review) is the author/funder, who has granted bioRxiv a license to display the preprint in perpetuity. It is made available under aCC-BY-NC-ND 4.0 International license.

52 **INTRODUCTION:**
53
54 mRNP granules are intriguing, dynamic membrane-less organelles containing translationally
55 repressed mRNAs, RNA-binding proteins (RBPs), molecular chaperones and a variety of other
56 cellular proteins (Buchan, 2014; Formicola *et al*, 2019; Kiebler & Bassell, 2006; Knowles *et*
57 *al*, 1996; Martin & Ephrussi, 2009). The formation and composition of mRNP assemblies are
58 determined by base-pairing interactions between mRNAs, protein-protein interactions and
59 RBP-RNA interactions, whose respective contributions may vary across granule types and
60 physiological states (Bevilacqua *et al*, 2022; Matheny *et al*, 2021; Van Treeck & Parker, 2018;
61 Van Treeck *et al*, 2018). Stress granules (SGs) are particularly well-studied granules that form
62 when cellular stress signals mediated by eIF2α kinase activation (Kedersha *et al*, 1999) cause
63 individual mRNPs to arrest in translation and condense into multi-mRNP assemblies (Ivanov
64 *et al*, 2019; Kedersha & Anderson, 2007; Youn *et al*, 2019). Mutations in mRNP granule
65 proteins, including TDP-43, FUS, Ataxin-2, hnRNPA1, hnRNPA2B1, EWSR1, have been
66 associated with ALS and/or other forms of neurodegenerative disease (Cirulli *et al*, 2015;
67 Couthouis *et al*, 2012; Elden *et al*, 2010; Ginsberg *et al*, 1998; Kim *et al*, 2013; Liu *et al*, 2017;
68 Taylor *et al*, 2016; Wolozin & Ivanov, 2019). For this reason, and because TDP-43 and other
69 stress-granule protein aggregates are components of protein inclusions found in ALS and
70 Frontotemporal dementia (FTD), the regulation and cellular functions of stress granules have
71 been topics of considerable fundamental and clinical interest (Cao *et al*, 2020; Li *et al*, 2013;
72 Mallucci *et al*, 2020; Protter & Parker, 2016; Wang *et al*, 2020; Wheeler *et al*, 2016; Wolozin
73 & Ivanov, 2019).
74
75 The cast of intermolecular interactions required for mRNP-granule assembly and the precise
76 sequence with which they occur are not yet elucidated (Khong & Parker, 2020; Van Treeck &
77 Parker, 2018). However, many studies show that intrinsically disordered regions (IDRs) found
78 on mRNP-granule proteins contribute substantially to RNP granule assembly (Andrusiak *et al*,
79 2019; Ash *et al*, 2021; Calabretta & Richard, 2015; Decker *et al*, 2007; Gilks *et al*, 2004;
80 Järvelin *et al*, 2016; Kim *et al*, 2021; Yang *et al*, 2020). In biochemical experiments, such IDRs
81 show the ability to phase separate into liquid-like assemblies (Babinchak & Surewicz, 2020;
82 Han *et al*, 2012; Hyman *et al*, 2014; Kato *et al*, 2012; Lin *et al*, 2017; Murray *et al*, 2017;
83 Murthy *et al*, 2019; Shin & Brangwynne, 2017; Strome & Wood, 1982; Toretsky & Wright,
84 2014; Yang *et al.*, 2020) The accessibility or activities of IDRs can be tightly regulated by
85 posttranslational modifications, allowing rapid physiological and spatial control over granule

bioRxiv preprint doi: https://doi.org/10.1101/2022.02.15.480566; this version posted February 17, 2022. The copyright holder for this preprint (which was not certified by peer review) is the author/funder, who has granted bioRxiv a license to display the preprint in perpetuity. It is made available under aCC-BY-NC-ND 4.0 International license.

86 assembly and disassembly (Ash *et al.*, 2021; Bah & Forman-Kay, 2016; Bah *et al*, 2015;
87 Berlow *et al*, 2015; Hofweber & Dormann, 2019; Kwon *et al*, 2013; Rayman *et al*, 2018; Saito
88 *et al*, 2019; Yang *et al.*, 2020).
89
90 An important observation is that most IDRs also have the ability to transition from liquid-like
91 states into solid, beta-sheet rich, amyloid-fibrils *in vitro*, particularly at high concentrations
92 achieved in the liquid-phase (Alberti *et al*, 2019; Li *et al.*, 2013; Murray *et al.*, 2017; Patel *et*
93 *al*, 2015; Ramaswami *et al*, 2013). This, and studies showing that inhibitors of eIF2α kinase or
94 downstream events including SG formation can be protective in animal models of
95 neurodegenerative disease (Chou *et al*, 2017; Halliday *et al*, 2017; Sidrauski *et al*, 2015; Wong
96 *et al*, 2018; Zyryanova *et al*, 2021) have led to a conceptual framework in which: (a) mRNP
97 granules provide a microenvironment where pathogenic protein seeds can form and grow
98 (Bakthavachalu *et al*, 2018; Mandrioli *et al*, 2020; Patel *et al.*, 2015); (b) increased misfolded-
99 protein loads result in inclusion formation, chronic stress signalling and reduced protein
100 translation (Hetz *et al*, 2020; Preissler & Ron, 2019); (c) increased demand on protein handling
101 systems results in multiple cellular defects, notably in the functions of membrane-less
102 organelles (Alberti *et al*, 2017; Azkanaz *et al*, 2019; Jiang *et al*, 2020; Latonen, 2019; Schuller
103 *et al*, 2021). In particular, aberrant SG formation also results in nuclear transport defects which
104 may contribute to cell death and toxicity (Hochberg-Laufer *et al*, 2019; Zhang *et al*, 2018).
105
106 Particularly strong support for the role of RNP granule formation in promoting disease comes
107 from studies of Ataxin-2. Loss of Ataxin-2 is cytoprotective in yeast TDP-43 and *Drosophila*
108 TDP-43 or C9ORF72 or Tau models of cytotoxicity (Bakthavachalu *et al.*, 2018; Becker *et al*,
109 2017; Elden *et al.*, 2010; Huelsmeier *et al*, 2021; Kim *et al*, 2014; Lee *et al*, 2016; Shulman &
110 Feany, 2003). In mouse models for SCA2 or ALS, either genetic loss of *ATXN2* or delivery of
111 antisense oligonucleotides (ASOs) targeting *ATXN2* in the central nervous system, reduced
112 aggregation of TDP-43, increased animal survival and improved motor function (Becker *et al.*,
113 2017; Scoles *et al*, 2017). These observations have led to ASOs against human *ATXN2* being
114 developed and approved for clinical trials (Biogen, 2021).
115
116 Given Ataxin-2's therapeutic significance and multiple roles in biology, it is particularly
117 important to determine which molecular activities of the protein are relevant to disease and to
118 its various biological functions (Kim *et al*, 2020). Across species, Ataxin-2 has three conserved
119 regions: a Like-Sm (LSm) domain, an LSm-associated domain (LSm-AD) and a PAM2 motif,

bioRxiv preprint doi: https://doi.org/10.1101/2022.02.15.480566; this version posted February 17, 2022. The copyright holder for this preprint (which was not certified by peer review) is the author/funder, who has granted bioRxiv a license to display the preprint in perpetuity. It is made available under aCC-BY-NC-ND 4.0 International license.

120 which is flanked by extended intrinsically disordered regions (IDRs) (Boeynaems *et al*, 2021).
121 Detailed work in *Drosophila* has shown that a c-terminal IDR of Atx2 is selectively required
122 for mRNP assembly into granules (Bakthavachalu *et al.*, 2018). Parallel experiments showing
123 that the IDR is also required for cytotoxicity in *Drosophila* FUS, C9ORF72 and Huntington's
124 disease models suggest RNP-granule formation to be a significant mechanism by which Atx2
125 promotes neurodegeneration (Bakthavachalu *et al.*, 2018; Huelsmeier *et al.*, 2021). A recent
126 discovery that the Atx2-LSm domain antagonizes IDR-function has led to a model in which
127 the Atx2 cIDR: (a) does not support mRNP assembly when Atx2 is associated with actively
128 translating mRNAs through Atx2-LSm domain interactions; (b) becomes accessible and active
129 in mediating mRNP assembly when LSm-domain interactions break and mRNA translation
130 stalls (Boeynaems *et al.*, 2021; Singh *et al*, 2021).
131
132 We now present a series of experiments further elaborating mechanisms by Ataxin-2 functions
133 in mRNA translation and mRNP assembly. These show that the PAM2 motif of Ataxin-2 and
134 its interactions with PABP are not essential for granule assembly but are required to efficiently
135 recruit Atx2-target mRNAs and specific protein components into Ataxin-2 granules. When
136 taken together with other findings (Boeynaems *et al.*, 2021; Kim *et al.*, 2014; Satterfield &
137 Pallanck, 2006; Singh *et al.*, 2021), our observations indicate that PAM2 binding to PABP on
138 the polyA tail of mRNAs helps specify the composition of Ataxin-2 granules. We propose an
139 early role for PAM2:PABP interactions working in coordination with the LSm domain to
140 support mRNA translation and thereby oppose the mRNP formation (Boeynaems *et al.*, 2021);
141 as well as a later role in escorting translationally-stalled PAM2:PABP linked mRNAs into
142 mRNP granules. *In vivo* experiments analysing motor decline in transgenic *Drosophila* indicate
143 that the PAM2:PABP interactions also support the progression of the neurodegenerative
144 process. We provide new evidence for fresh insight into the enigmatic role of mRNP assembly
145 in neurodegeneration.
146

147 **RESULTS:**

148

149 ***The structured PAM2 domain of Atx2 is necessary for the correct mRNA and protein content***
150 ***of Atx2 granules.***

151
152 A recent eLife publication used Targets of RNA-Binding Proteins Identified by Editing
153 (TRIBE) technology to identify mRNAs associated with Atx2 in the *Drosophila* adult brain

bioRxiv preprint doi: https://doi.org/10.1101/2022.02.15.480566; this version posted February 17, 2022. The copyright holder for this preprint (which was not certified by peer review) is the author/funder, who has granted bioRxiv a license to display the preprint in perpetuity. It is made available under aCC-BY-NC-ND 4.0 International license.

154 (Singh *et al.*, 2021). *In vivo*, the ability of an Atx2-fusion with ADARcd (the catalytic domain
155 of an RNA-editing enzyme, ADAR), to edit a group of 256 target mRNAs was found to be
156 dependent on the presence of the Atx2-cIDR, previously shown to be necessary for the
157 formation of neuronal mRNP granules *in vivo*. In contrast, Atx2-ADARcd mutants lacking the
158 LSm domain, both edited Atx2 TRIBE target RNAs and formed mRNP granules in cultured
159 *Drosophila* S2 cells more efficiently than the wild-type. Thus, Atx2-ADARcd editing of target
160 mRNAs occurs in and is reflective of mRNP granule assembly. While demonstrating a role for
161 LSm-domain interactions in antagonizing cIDR mediated granule assembly, these observations
162 did not address mechanisms by which Atx2 target mRNAs are selected, or whether and how
163 Atx2 played any role in determining the composition of RNP granules. New experiments
164 presented here address these outstanding questions.
165
166 Previous TRIBE analyses showed that LSm and LSm-AD regions have no major role in the
167 recognition or selection of the Atx2-target mRNAs (Singh *et al.*, 2021). We therefore tested
168 whether the third conserved region of Ataxin-2, a PAM2 motif known to associate with PABP
169 (polyA binding protein), played any role in this process (Jiménez-López & Guzmán, 2014;
170 Kaehler *et al*, 2012).
171
172 We used Gal80^{ts}-controlled *elav-Gal4* to express Atx2ΔPAM2-ADARcd (deleted for the
173 PAM2 motif) in brains of adult *Drosophila* for 5 days and used RNA-Seq to identify edited
174 RNAs in polyA selected brain mRNA and compare it with Atx2-ADARcd using procedures
175 described earlier (Figure 1A) (McMahon *et al*, 2016). ADAR-edits, which converts Adenosine
176 to Inosine on RNAs, are identified as A to G changes in TRIBE analyses. Each sample was
177 sequenced to obtain 20 million reads (Supplementary table 1). The edits were only considered
178 from the regions of the transcriptome that contained at least 20 reads. Genes with edits
179 identified at a threshold above 15% in two biological replicates were considered as high-
180 confidence true targets. We compared edit frequency and edited-gene identity in the brains of
181 flies expressing Atx2ΔPAM2-ADARcd with those in brains expressing Atx2-ADARcd.
182
183 In contrast to Atx-2 forms lacking LSm or LSm-AD domains (Singh *et al.*, 2021),
184 Atx2ΔPAM2-ADARcd edited significantly fewer RNA targets than wild-type Atx2-ADARcd
185 (108 genes and 165 edits vs 256 genes and 317 edits, Figure 1B, C and Supplementary table
186 2). More striking, the cohort of mRNAs edited by the ΔPAM2 mutant form differed extensively
187 from the largely overlapping cohorts edited by either wild-type forms of Atx2 (Figure 1C). Of

bioRxiv preprint doi: https://doi.org/10.1101/2022.02.15.480566; this version posted February 17, 2022. The copyright holder for this preprint (which was not certified by peer review) is the author/funder, who has granted bioRxiv a license to display the preprint in perpetuity. It is made available under aCC-BY-NC-ND 4.0 International license.

188 the 108 genes edited by Atx2ΔPAM2-ADARcd, 36 were also targets of Atx2-ADARcd, the
189 remaining 72 were unique. (Figure 1C, D and Supplementary table 2). 50 edit sites were
190 common between the Atx2ΔPAM2 and Atx2WT targets. Those sites were edited with much
191 lower efficiency in Atx2ΔPAM2 as compared to Atx2WT (Figure 1E).
192
193 The location of edits made by Atx2ΔPAM2-ADARcd also differed dramatically as to where
194 they occurred relative to the coding sequences of the target mRNAs (Figure 1F). While edits
195 made by wild-type and ΔLSm forms of Atx2-ADARcd were greatly enriched in the 3'UTR of
196 the mRNAs, Atx2ΔPAM2 targets were edited indiscriminately all along the mRNA length
197 (Figure 1F).
198
199 Taken together, these data identify the PAM2 motif as necessary for Atx2 engagement with its
200 correct mRNA targets. The PAM2 motif interacts with PABP, which binds polyA tracts at the
201 3' end of mRNAs (Deo *et al*, 1999). Therefore, the data point to a role for the structured
202 PAM2:PABP interaction in guiding the association of Atx2 with mRNAs and for subsequent
203 inclusion of these mRNAs in Atx2-containing granules.
204
205 If Atx2-ADARcd edits of target mRNAs occur predominantly in the mRNP granules (Singh *et*
206 *al.*, 2021), then the ability of Atx2ΔPAM2-ADARcd to edit some target mRNAs would suggest
207 that the PAM2 motif is not essential for mRNP granule formation *per se.* To examine this, we
208 expressed wild-type and ΔPAM2 mutant forms of GFP-tagged Atx2 under control of the native
209 genomic promoter in *Drosophila* S2R+ cells. Atx2 overexpression in S2 cells induced the
210 formation of mRNP granules closely related to SGs, containing endogenous Atx2 and various
211 SG proteins as previously reported (Figure 2A) (Bakthavachalu *et al.*, 2018; Singh *et al.*, 2021).
212 Similar expression of Atx2ΔPAM2-GFP also induced granule formation. However, these
213 granules were compositionally distinct from those induced by Atx2-GFP. While they clearly
214 contained some SG markers present on Atx2-granules, e.g., Me31B and Rox8 (*Drosophila*
215 homologs of DDX6 and TIA1), they did not contain others such as PABP, Caprin and dFMRP
216 (Figure 2B).
217
218 RNP-granules induced by expression of wild-type, LSm and PAM2 deficient forms of Atx2-
219 GFP required the presence of the c-terminal IDR (Figure 2C). Thus, while largely dispensable
220 for efficient mRNP assembly, the PAM2 domain plays a significant role in determining both
221 mRNA and protein components of mRNP granules. One possibility is that the PAM2 motif

bioRxiv preprint doi: https://doi.org/10.1101/2022.02.15.480566; this version posted February 17, 2022. The copyright holder for this preprint (which was not certified by peer review) is the author/funder, who has granted bioRxiv a license to display the preprint in perpetuity. It is made available under aCC-BY-NC-ND 4.0 International license.

222 directly recruits PABP and associated mRNAs to granules and indirectly recruits other proteins
223 through their interactions with either PABP or mRNAs brought to RNP granules through Atx2-
224 PAM2:PABP interactions.

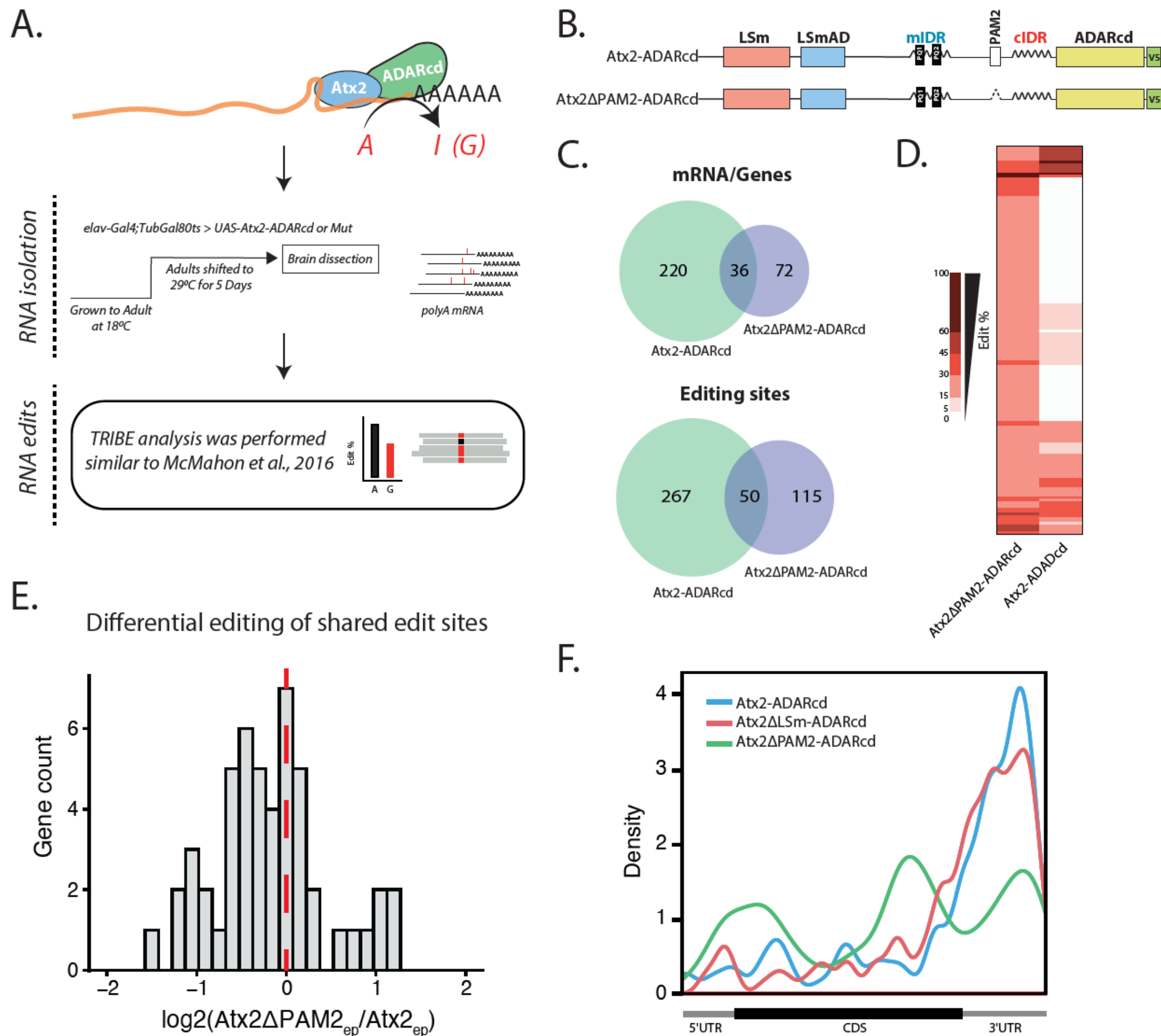

225

226 **Figure 1: The PAM2 domain facilitates the selection of Atx2 RNA targets.** (A). Flowchart depicting
227 the TRIBE analyses pipeline. Atx2ΔPAM2-ADARcd was expressed in adult *Drosophila* brains. Total
228 brain RNA was isolated and RNA edits were identified and compared to Atx2-ADARcd, similar to Singh
229 et al 2021. (B) Domain map of Atx2-ADARcd constructs used for TRIBE analysis. (C) Comparisons of
230 genes and edits identified by TRIBE between Atx2-ADARcd and Atx2ΔPAM2-ADARcd targets. (D)
231 Most Atx2ΔPAM2 targets identified by TRIBE are unique and not edited in Atx2WT, suggesting that
232 these new targets bound by Atx2ΔPAM2 are not native Ataxin-2 granule targets. (E) Comparisons of the
233 editing efficiency ratio of common edits between Atx2WT vs Atx2ΔPAM2 show a much lower editing
234 efficiency in Atx2ΔPAM2 compared to Atx2WT. (F) PAM2 deletion results in loss of 3'UTR specificity
235 seen in Atx2WT and LSm deletion TRIBE target mRNAs. Atx2WT and Atx2ΔLSm-ADARcd data are
236 extracted from (Singh et al 2021).

bioRxiv preprint doi: https://doi.org/10.1101/2022.02.15.480566; this version posted February 17, 2022. The copyright holder for this preprint (which was not certified by peer review) is the author/funder, who has granted bioRxiv a license to display the preprint in perpetuity. It is made available under aCC-BY-NC-ND 4.0 International license.

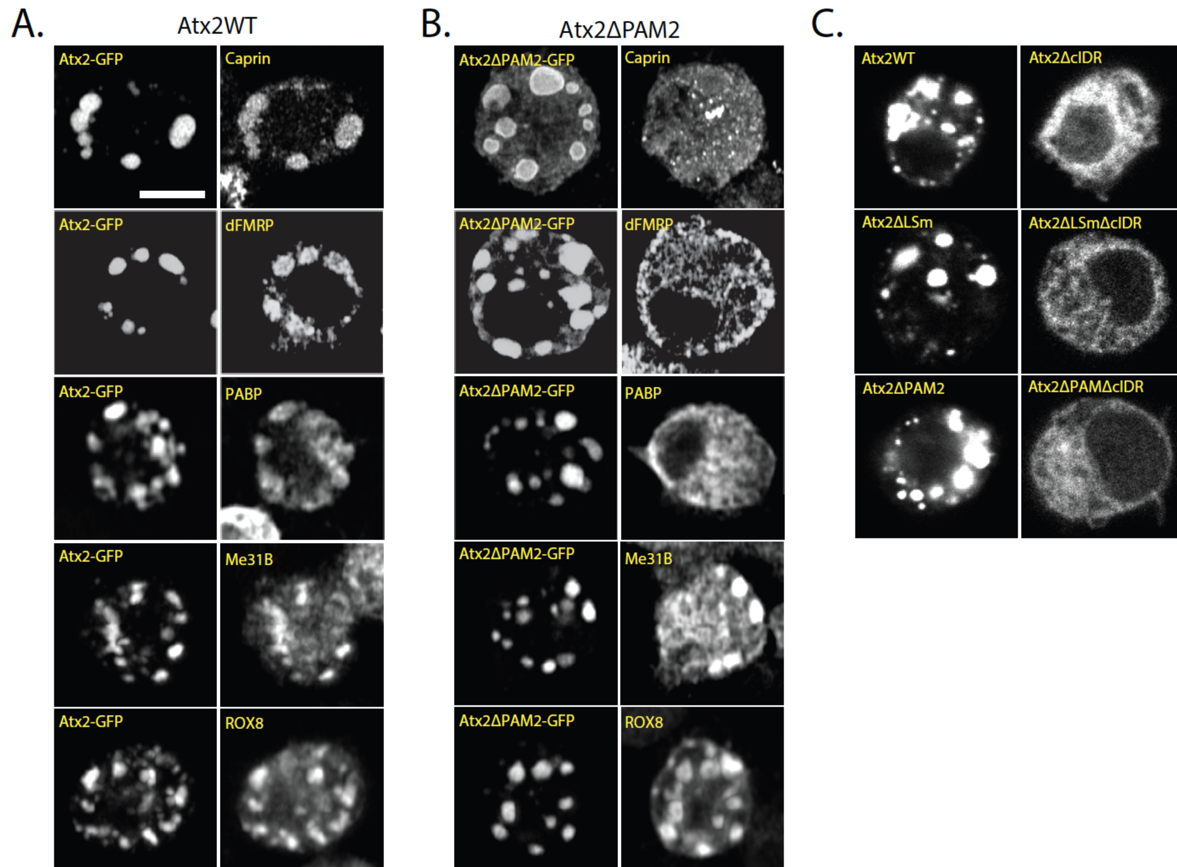

237

238 **Figure 2: Presence of the PAM2 domain affects the protein composition of Atx2-GFP granules in S2**
239 **cells.** (A) Over-expression of Atx2-GFP in unstressed *Drosophila* S2 cells induces the formation of Atx2-
240 GFP granules to which various SG markers co-localize. (B) Deletion of the PAM2 affects the Atx2-GFP
241 granule composition. Over-expression of Atx2ΔPAM2-GFP in S2 cells still induces the formation of
242 granules, but some SG markers fail to co-localize in these, notably dFMR, Caprin and PABP. (C) Atx2-
243 GFP granule formation in S2 cells relies primarily on the cIDR. Deletion of the cIDR in Atx2WT,
244 Atx2ΔPAM2 and Atx2ΔLSm, removes their ability to form granules upon overexpression. See
245 Supplemental Figure 1, A-B, for quantification. The scale bar in (A) applies to (B) and (C). Scale bar = 5
246 µm,

247

248 ***PAM2:PABP interactions are sufficient for Atx2 to associate with stress granules***

249 We wanted to directly confirm Ataxin-2 PAM2 motif interactions with PABP and analyse their
250 relevance to RNP granule assembly. For this, we generated constructs encoding SNAP-epitope
251 tagged variants of Atx2. These were radically truncated forms of *Drosophila* and human
252 Ataxin-2 proteins containing only the LSm, LSm-AD and PAM2 elements and lacking all
253 unstructured regions of the protein. The structured elements are connected via flexible linkers
254 (Figure 3A). These "Mini-Ataxin-2" constructs and their domain-deleted forms allowed us to
255 separate functions of the structured regions of Ataxin-2 from those of the remaining extended

bioRxiv preprint doi: https://doi.org/10.1101/2022.02.15.480566; this version posted February 17, 2022. The copyright holder for this preprint (which was not certified by peer review) is the author/funder, who has granted bioRxiv a license to display the preprint in perpetuity. It is made available under aCC-BY-NC-ND 4.0 International license.

256 disordered regions. A similar approach has been previously shown for MeCP2 (Tillotson *et al*,
257 2017). We identified key residues involved in *Drosophila* Atx2-PAM2:PABP interactions
258 based on a previously solved crystal structure of a strongly conserved mammalian
259 PAM2:PABPC1-MLLE domain complex (Kozlov *et al*, 2010; Xie *et al*, 2014) (Figure 3B).
260 Residues leucine 914 and phenylalanine 921 (L914 and F921) in the human ATXN2-PAM2
261 motif are predicted to contact the PABPC-MLLE domain and of these, F921 has been shown
262 to be required for the PABPC-ATXN2 interaction (Inagaki *et al*, 2020). These residues (L859
263 and F866, respectively) are perfectly conserved in fly Atx2 (Supplementary Figure 3). In order
264 to allow more precise disruption of PAM2:PABP interactions and avoid potential unknown
265 secondary effects of larger PAM2 motif deletions, we additionally generated mini Ataxin-2
266 constructs where these PABP-contacting residues were singly or doubly altered to alanine. We
267 used these constructs for co-immunoprecipitation (Figure 3) and co-localization (Figure 4)
268 analyses to examine the contribution of PAM2:PABP/PABPC1 interactions in RNP-granule
269 formation.
270
271 We expressed SNAP-tagged wild-type and mutant forms of mammalian and *Drosophila* mini-
272 Ataxin-2 in HEK293T and S2 cells, respectively. We tested which Ataxin-2 domains were
273 required for SNAP substrate beads to successfully immunoprecipitate Ataxin-2 complexes
274 containing PABPC1/PABP from cell lysates (Figure 3C-E). Both LSM12 and PABPC1
275 proteins were co-immunoprecipitated with mammalian mini-ATXN2. However, PABPC1 co-
276 immunoprecipitation was selectively lost when the PAM2 domain was deleted or if predicted
277 PABP-contact residues in the PAM2 domain were mutated (Figure 3C). Similar to the human
278 homolog, fly mini-Atx2-SNAP also required the presence of its PAM2 motif with both
279 predicted contact residues intact for immunoprecipitation of PABP from *Drosophila* S2 cell
280 lysates (Figure 3D). Taken together with previous observations, these data support a potential
281 sequence of molecular events. In unstressed cells, PAM2 domain interaction with PABP help
282 position Ataxin-2 at the 3’-end of mRNAs while LSM-domain association with LSM12
283 stimulate translation of these mRNAs; under stress conditions (or Ataxin-2 overexpression),
284 translation is arrested and the cIDR domain freed to mediate interactions that facilitate the
285 formation of condensed RNP granules (see Discussion)

bioRxiv preprint doi: https://doi.org/10.1101/2022.02.15.480566; this version posted February 17, 2022. The copyright holder for this preprint (which was not certified by peer review) is the author/funder, who has granted bioRxiv a license to display the preprint in perpetuity. It is made available under aCC-BY-NC-ND 4.0 International license.

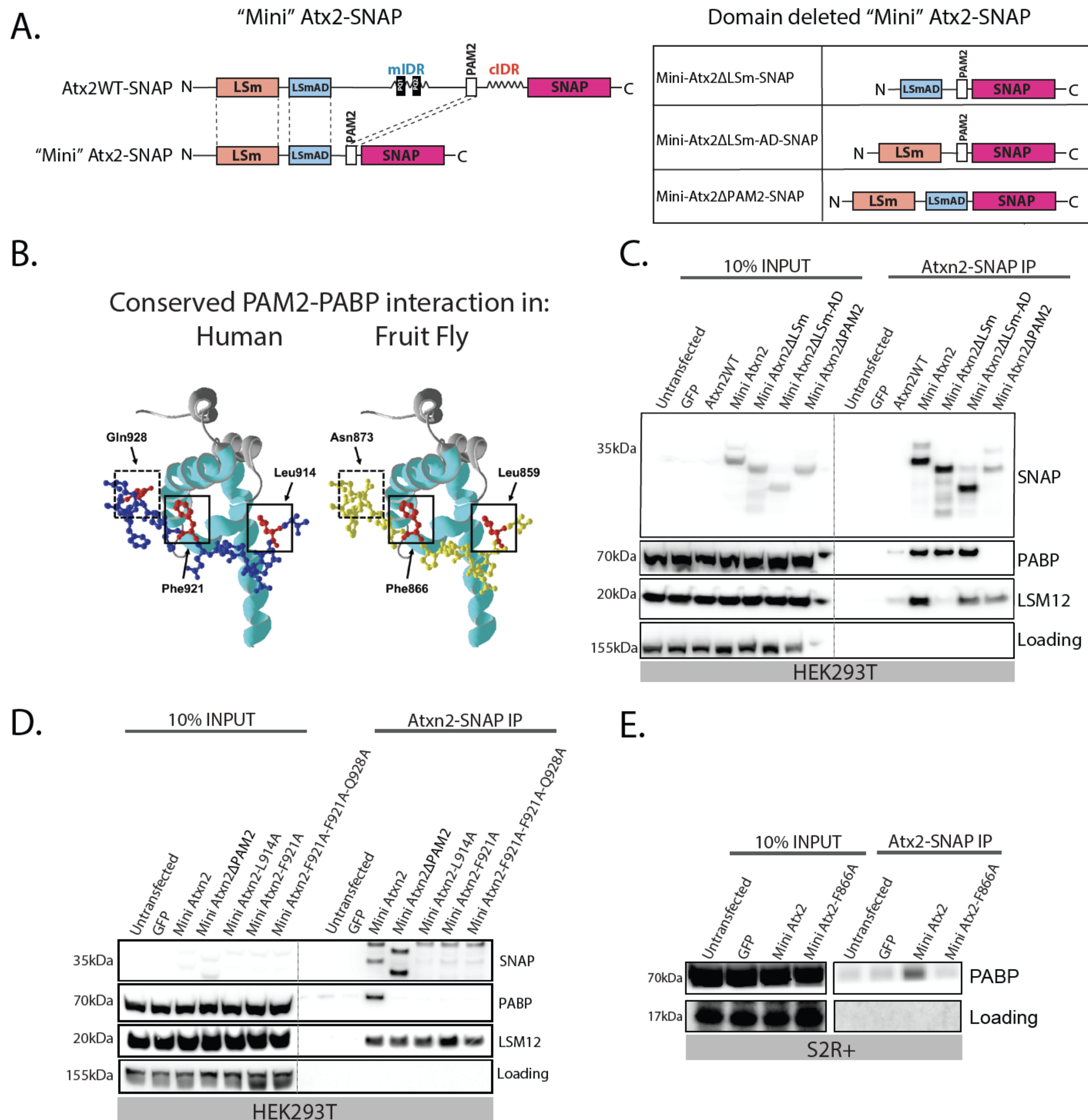

286

287 **Figure 3: A minimized Ataxin-2 construct containing only the known structured domains maintains**
288 **the ability to interact with PABP and LSM12.** (A) Schematic of SNAP-tagged full length, minimal, and
289 minimal domain-deleted constructs of fly Atx2 used to isolate the function of the structured domains of the
290 protein without interference from IDR-mediated interactions. Human and *Drosophila* Ataxin-2 LSm, LSm-
291 AD and PAM2 domains show high amino acid sequence similarity (Clustal Ω) of 70%, 82% and 87%
292 respectively. This suggests conserved and specific function of these structured domains. (B) Structural
293 model of the PABP MLLE domain (ribbon) showing the near-perfect structural similarity of the human
294 ATXN2 PAM2 domain (blue, uniprot ID: Q99700) with the *Drosophila* Atx2 PAM2 domain (yellow,
295 uniprot ID: Q8SWR8). The key interacting residues are highlighted in red. (C) Human minimized
296 ATXN2 SNAP IP-WB from HEK293T cells probing for PABP and LSM12 showing the effects of
297 different domain deletions. The PAM2 domain is necessary and sufficient for the ATXN2-PABP
298 interaction, while the LSm domain is necessary and sufficient for the ATXN2-LSM12 interaction. (D)
299 Point-mutations targeting key interacting residues of the PAM2 domain were predicted to replicate the

bioRxiv preprint doi: https://doi.org/10.1101/2022.02.15.480566; this version posted February 17, 2022. The copyright holder for this preprint (which was not certified by peer review) is the author/funder, who has granted bioRxiv a license to display the preprint in perpetuity. It is made available under aCC-BY-NC-ND 4.0 International license.

300 effect of a full PAM2 deletion in the minimized Atx2 construct. Human minimized ATXN2-SNAP IP
301 WB from HEK293T cells showing that mutating either of the key hydrophobic residues L914 or F921 in
302 the PAM2 domain is sufficient to prevent its interaction with PABP. The interaction with LSM12 is
303 unaffected by the point mutations. (E) *Drosophila* minimized Atx2-SNAP IP-WB from S2 cells. An
304 analogous PAM2 domain point mutation on F866 blocks the Atx2-PABP interaction.
305
306 Single mRNAs usually associate with multiple PABP molecules because their polyA tails are
307 considerably longer than the ~24 bases required for PABP binding (Mangus *et al*, 2003). Thus,
308 in cells expressing endogenous and mini Ataxin-2, mRNAs could have both forms associated
309 with their polyA tails. In response to stress, mini Ataxin-2 would be expected to move into SGs
310 whose formation is facilitated by IDRs on endogenous Ataxin-2 associated with the common
311 target RNAs. We examined this possibility in cells before and after oxidative stress.
312
313 *Drosophila* and human mini-Ataxin-2-SNAP, expressed in fly S2 or human U2OS cells
314 respectively, were diffusely localized in the cytoplasm and neither induced formation of
315 Ataxin-2 foci. However, when cells were exposed to sodium arsenite to induce SG formation,
316 SNAP-tagged mini-Atx2 (Figure 4A) and mini- ATXN2 (Figure 4H) were robustly recruited
317 to stress granules. Thus, association of Ataxin-2 with mRNP-granule components may be
318 achieved by structured domain interactions alone, independently of IDRs required for mRNP
319 assembly into granules.
320
321 Further experiments examined which of the LSm, LSm-AD and/or PAM2 domains were
322 necessary for mini-Ataxin-2 to associate with stress granules. Mammalian and *Drosophila*
323 mini-Ataxin-2 forms missing the LSm or LSm-AD domains could still be found in stress
324 granules (Figure 4B-C and I-J). In contrast, mutants lacking the PAM2 domain remained
325 cytoplasmic after stress in both S2 (Figure 4D) and U2OS cells (Figure 4K). Notably, point
326 mutations in the Ataxin-2-PAM2 domain that specifically disrupt PAM2:PABP interaction
327 similarly prevent localization to stress granules (Figure 4E-G and L-N). Thus, interactions
328 between Ataxin-2's PAM2 domain and PABP appear important for the presence of Ataxin-2
329 in native mRNP granules, whose assembly is driven by the distinct (IDR) region of the protein
330 (Figure 2C). The ability of otherwise full-length Ataxin-2 lacking PAM2 to form
331 compositionally distinct mRNP assemblies (Figure 2B) suggests that PAM2:PABP binding
332 also serves to limit non-physiological interactions by Ataxin-2 (See Discussion).
333

bioRxiv preprint doi: https://doi.org/10.1101/2022.02.15.480566; this version posted February 17, 2022. The copyright holder for this preprint (which was not certified by peer review) is the author/funder, who has granted bioRxiv a license to display the preprint in perpetuity. It is made available under aCC-BY-NC-ND 4.0 International license.

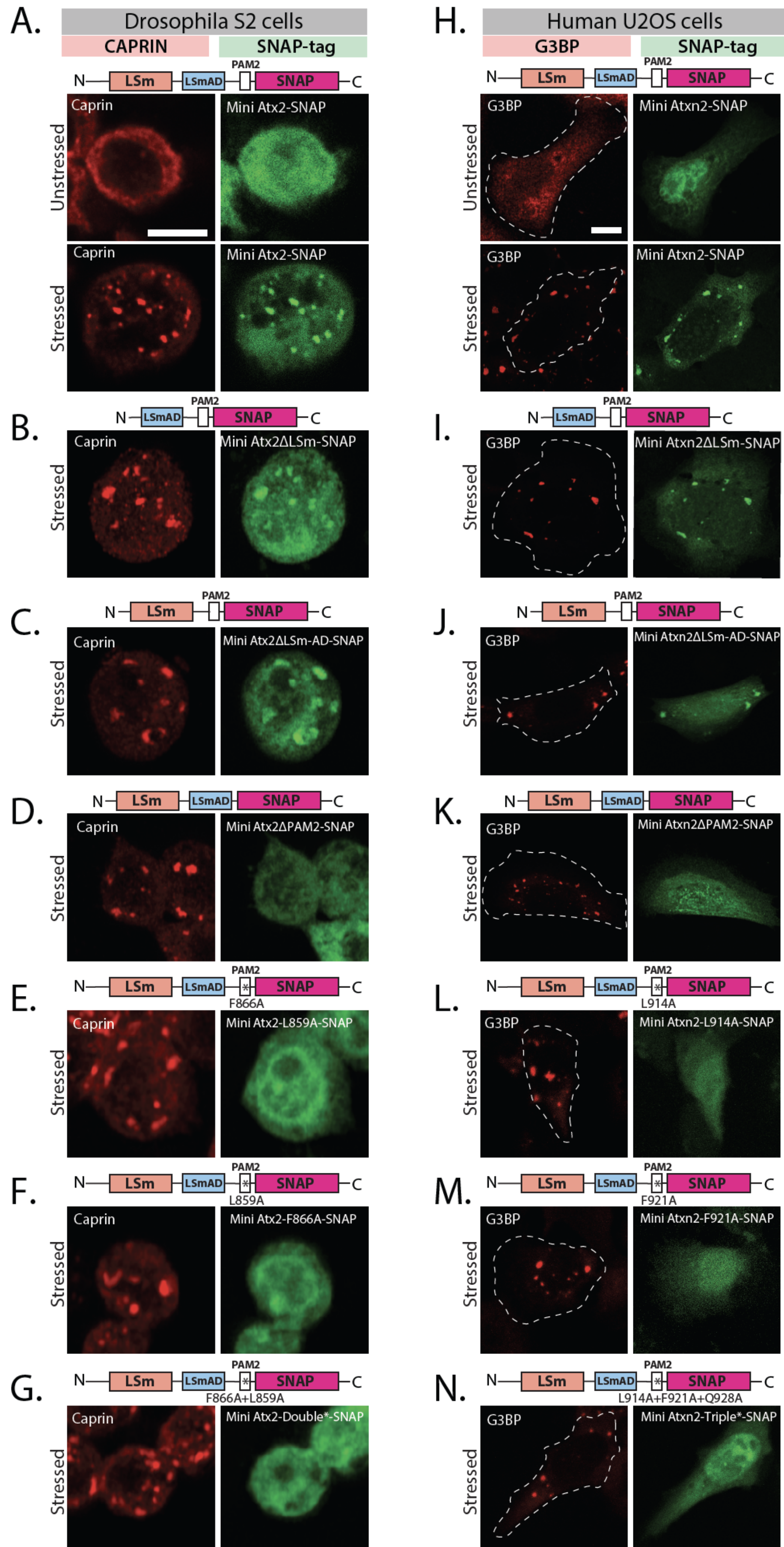

334

bioRxiv preprint doi: https://doi.org/10.1101/2022.02.15.480566; this version posted February 17, 2022. The copyright holder for this preprint (which was not certified by peer review) is the author/funder, who has granted bioRxiv a license to display the preprint in perpetuity. It is made available under aCC-BY-NC-ND 4.0 International license.

335 **Figure 4**: **The structured PAM2 domain is necessary and sufficient for Ataxin-2 recruitment to Stress**
336 **Granules in both *Drosophila* and human cells.** (A) In *Drosophila* S2 cells mini-Atx2-SNAP (green) is
337 recruited to SGs induced by arsenite. (B) Deletion of LSm or (C) LSm-AD domains has no significant
338 effect in the arsenite-induced SG recruitment. (D) The presence of PAM2 domain, and specifically its key
339 PABP-interacting amino acids (E-G), is necessary for Atx2 recruitment to SGs. Caprin (red) was used as
340 SG granule marker, scale bar = 5 µm, (H) Human mini-ATXN2-SNAP (green) is recruited to arsenite-
341 induced SGs in human U2OS cells. (I) Deletion of LSm or (J) LSm-AD domains has no effect on the
342 arsenite-induced SG recruitment of ATXN2. (K) Deletion of the PAM2 domain, and specifically its
343 PABP-interacting amino acids (L-N), are necessary for ATXN2 recruitment to SGs. G3BP1 (red) was
344 used as SG marker; scale bar = 10 µm. Schematics above images indicate the domain deletions or amino
345 acid mutations that were made in the different Ataxin-2 constructs. See Supplemental Figure 1C for
346 quantification.
347
348 ***The IDR and PAM2 domains promote and the LSm domain inhibits cytotoxicity in***
349 ***Drosophila neurodegeneration models.***
350
351 Three different Ataxin-2 domain deletions tested showed three distinct effects on mRNP
352 granule assembly in S2 cells. IDR domain deletions prevent Ataxin-2 granule formation. LSm-
353 domain deletion enhances the formation of Ataxin-2 granules. PAM2 domain deletions result
354 in the formation of unusual mRNP assemblies (Bakthavachalu *et al.*, 2018; Singh *et al.*, 2021)
355 (Figure 2B/C). Prior observations showing that Atx2 IDR deletions suppress cytotoxicity in
356 *Drosophila* models for neurodegeneration indicate that mRNP granules support events that
357 lead to degenerative disease (Bakthavachalu *et al.*, 2018; Becker *et al.*, 2017; Huelsmeier *et*
358 *al.*, 2021; Scoles *et al.*, 2017). If true, the expression of Atx2ΔLSm, which enhances granule
359 assembly, would promote or potentially accelerate the degeneration, while the expression of
360 Atx2ΔcIDR would not. The expression of Atx2ΔPAM2 would be expected to support mRNP
361 assemblies of different compositions from the ones containing wild-type or ΔLSm forms of
362 Atx2. The effects on degeneration for this condition would be hard to predict.
363
364 To examine how the different Atx-2 domain deletions affect nervous system integrity and
365 function over time, we combined a Gal4-responsive *UAS-Atx2* transgene with *elav-Gal4* and
366 *TubGal80*^{ts}. This allows us to use a temperature shift from 18ºC to 30ºC to induce *UAS-Atx2*
367 transgene expression, specifically in the brains of adult flies (Figure 5A). We then analysed the
368 rate at which flies climbed the walls of a glass cylinder, a surrogate measure of motor ability,
369 one day and 15 days after transgene expression. All genotypes tested showed robust and

bioRxiv preprint doi: https://doi.org/10.1101/2022.02.15.480566; this version posted February 17, 2022. The copyright holder for this preprint (which was not certified by peer review) is the author/funder, who has granted bioRxiv a license to display the preprint in perpetuity. It is made available under aCC-BY-NC-ND 4.0 International license.

370 comparable levels of climbing ability on day 1. Interesting variations were identified on day
371 15. The 15-day old flies expressing Atx2WT or Atx2ΔLSm showed a strong decline in
372 climbing ability. In contrast, Atx2 ΔcIDR flies showed a minimal decline (Figure 5B). These
373 observations were in line with the effects of these Atx2 types on granule formation. Strikingly,
374 flies expressing the Atx2ΔPAM variant, which formed compositionally distinct granules in S2
375 cells, showed no significant decline in climbing ability, suggesting that Atx2's ability to
376 promote progressive decline of neural function depends less on Atx2 granule formation and
377 aggregation, but a bit more on its sequestration of critical translation factors such as PABP (and
378 associated RNAs.(Figure 5B). These observations support and extend prior work showing that
379 heterologous overexpression of full-length, but not PAM2-domain deleted forms of
380 mammalian ATXN2 enhances mammalian TDP-43-induced degeneration of the *Drosophila*
381 compound eye (Kim *et al.*, 2014). They are also consistent with work in mice showing that
382 PABPC1 sequestration in inclusions correlates strongly with the progression of
383 neurodegeneration (Damrath *et al*, 2012).
384
385 The conclusion, that PAM2 mediated interactions were required for progressive cytotoxicity,
386 is further supported by a parallel series of experiments in which we used *mef2-Gal4* in place
387 of *elav-Gal4,* to *target UAS-Atx2* transgene expression to *Drosophila* adult muscles (Figure
388 5C). Micro-computed tomography (micro-CT) scanning to visualize the integrity of flight
389 muscle fibers in whole-mount preparations (see Methods) revealed degeneration of muscles
390 expressing wild-type Atx2 in 20-day old flies. While there was more severe degeneration in
391 Atx2ΔLSm expressing muscle, muscles similarly expressing Atx2ΔcIDR or Atx2ΔPAM forms
392 showed no morphological defects (Figure 5C and Supplementary Figure 4).

bioRxiv preprint doi: https://doi.org/10.1101/2022.02.15.480566; this version posted February 17, 2022. The copyright holder for this preprint (which was not certified by peer review) is the author/funder, who has granted bioRxiv a license to display the preprint in perpetuity. It is made available under aCC-BY-NC-ND 4.0 International license.

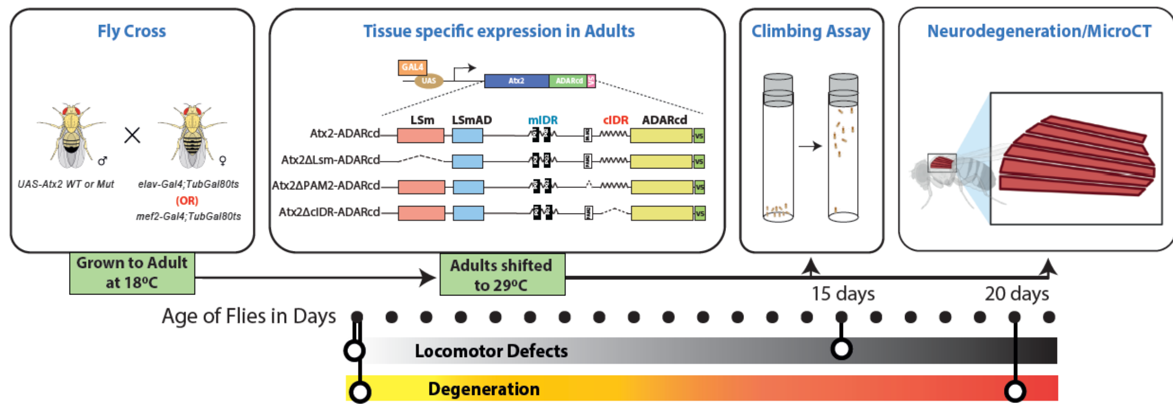

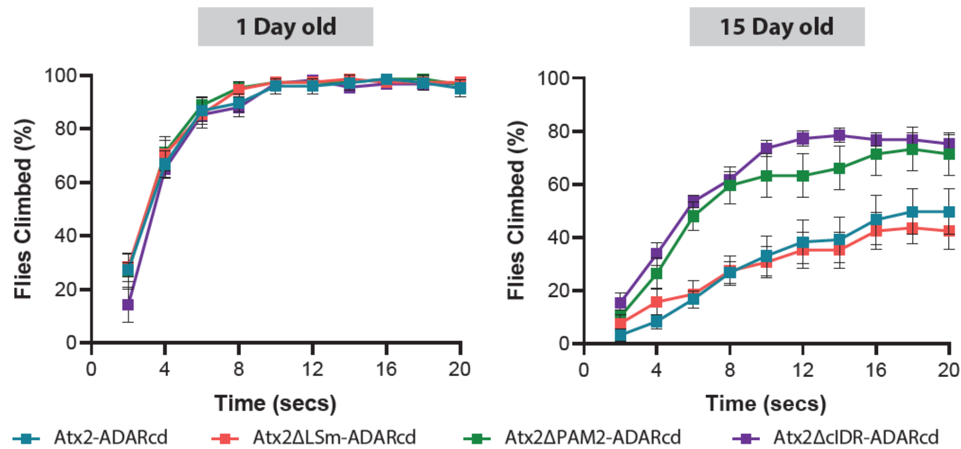

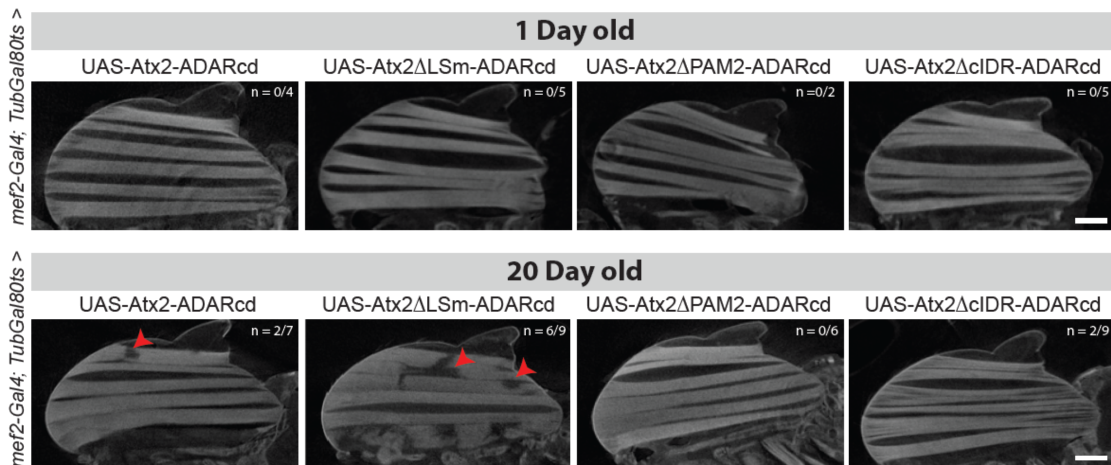

Figure 5: The IDR and PAM2 domains promote and the LSm domain inhibits neurodegeneration in *Drosophila*. (A) A schematic of the experimental design is shown. UAS-transgenes were crossed with *elav-Gal4; tub-Gal80^{ts}* or *mef2-Gal4, tub-Gal80^{ts}* and kept at 18°C till the adult flies emerged. The flies were shifted to 29 °C for days shown with dots under the experimental design. Fly climbing or indirect flight muscle cytotoxicity was studied. (B) *Drosophila* climbing behavior assay was performed by driving UAS-transgene (Atx2WT, Atx2ΔcIDR, Atx2ΔPAM or Atx2ΔLSm) with *elav-Gal4.* A graph was plotted with number of flies (Y-axis) that crossed the 20ml mark at a given time (X-axis). (C) Cellular toxicity was measured by driving UAS-transgene (Atx2WT, Atx2ΔcIDR, Atx2ΔPAM or Atx2ΔLSm) with *mef2-*

bioRxiv preprint doi: https://doi.org/10.1101/2022.02.15.480566; this version posted February 17, 2022. The copyright holder for this preprint (which was not certified by peer review) is the author/funder, who has granted bioRxiv a license to display the preprint in perpetuity. It is made available under aCC-BY-NC-ND 4.0 International license.

402 *Gal4*. Fly indirect flight muscles were imaged using micro-CT and the loss of muscle fibers is shown with
403 solid red arrowheads.
404

405 ## DISCUSSION

406 The results described above provide three significant lines of insight. First, they support a
407 detailed model for sequential protein-protein interactions through which Ataxin-2 can
408 modulate different translational states of a single mRNA. Second, they show that the Ataxin-2
409 polypeptide contains distinct activities that promote or protect against neurodegeneration,
410 pointing to the value of developing therapeutics that target specific Ataxin-2 interactions,
411 beyond those that reduce overall levels of the protein. Third, the work identifies a novel
412 molecular mechanism involving the PAM2 domain and PABP that contributes to the assembly
413 of mRNP granules.
414

415 ### Molecular mechanisms of Ataxin-2 function

416 Some RNA-binding proteins can remain associated with mRNAs across multiple stages: RNA
417 processing, transport, translation, or translational control (Formicola *et al.*, 2019; Gomes &
418 Shorter, 2019; Hachet & Ephrussi, 2004; Harlen & Churchman, 2017; Lin *et al*, 2015; Maniatis
419 & Reed, 2002). Ataxin-2 may be one such protein. It is a translational activator of the
420 *Drosophila period* mRNA, a repressor of several miRNA reporters, a facilitator of neuronal
421 mRNP-granule and stress-granule formation as well as a broad stabilizer of Ataxin-2 associated
422 mRNAs (Bakthavachalu *et al.*, 2018; Inagaki *et al.*, 2020; Lim & Allada, 2013; McCann *et al*,
423 2011; Nonhoff *et al*, 2007; Sudhakaran *et al*, 2014; Yokoshi *et al*, 2014; Zhang *et al*, 2013).
424 While these different functions could represent different modes of engagement with distinct
425 sets of mRNAs, the data are also consistent with another model. Sequential interactions
426 mediated by different protein regions during mRNP modelling allow Ataxin-2 to contribute in
427 multiple ways to translational control to a single mRNA.
428

429 Previous work has shown that Atx-2 enhances *period* mRNA translation through a mechanism
430 requiring LSm-domain interactions with a complex of LSM12 and TYF (Twenty Four) proteins
431 associated with the 5'cap of the translating mRNA (Lee *et al*, 2017; Lim & Allada, 2013; Zhang
432 *et al.*, 2013). Given considerable supportive evidence for direct binding between the LSm-
433 domain and LSM12, we postulate that LSm-domain-LSM12 interactions occur in translating
434 polysomes (Satterfield & Pallanck, 2006) and contribute to increased efficiency of translation.

bioRxiv preprint doi: https://doi.org/10.1101/2022.02.15.480566; this version posted February 17, 2022. The copyright holder for this preprint (which was not certified by peer review) is the author/funder, who has granted bioRxiv a license to display the preprint in perpetuity. It is made available under aCC-BY-NC-ND 4.0 International license.

435 This proposal is consistent with the observation that the LSm domain opposes the formation of
436 mRNP granules, which usually contain translationally repressed mRNAs (Singh *et al.*, 2021).
437
438 However, the LSm domain must also contribute to LSM12-independent functions, because
439 while LSm-domain deletions from *Drosophila* Atx2 cause lethality and LSM12 null mutants,
440 while arrhythmic, are viable and fertile (Lee *et al.*, 2017). One possibility is that LSm domains
441 additionally contribute, perhaps indirectly, to interactions with the DEAD-box helicase
442 Me31B/DDX6 in a translational repressor complex (Brandmann *et al*, 2018; Lee *et al.*, 2017).
443 Thus, we suggest that in the case of actively translating mRNAs, the Atx2 function is driven
444 by LSm-domain association with LSM12 and translational initiators, and that LSM12
445 disengages from a translational initiation complex as the mRNA transitions into a repressed
446 state driven by Me31B.
447
448 While polyA tails and PABP are known to support translation and the Ataxin-2 PAM2 domain
449 is involved in targeting the protein to polysomes (Satterfield and Pallanck, 2006), existing data
450 do not directly address how Ataxin-2 PAM2 motif interactions contribute to translational
451 activation. One possibility, supported by observations on the *period* mRNA is that the PAM2-
452 domain guides Ataxin-2 to the 3'UTR of its target mRNAs (Lim & Allada, 2013). Our
453 observation that PABP co-immunoprecipitates with mini-Ataxin2, show that Atx2-
454 PAM2:PABP interactions occur independently of and prior to mRNP granule formation.
455 Recent findings that this association antagonizes the Ataxin-2 condensation (Boeynaems *et al.*,
456 2021) are consistent with a model in which the Atx2-PAM2 motif interacts with PABP in
457 translating mRNAs to support efficient translation driven by the LSm-LSM12 complex.
458 However, in addition to supporting translation, PABP is also known to associate with
459 translational repressors that could drive either mRNA deadenylation and/or storage (Machida
460 *et al*, 2018; Yoshida *et al*, 2006). Our data support such a dual role for Ataxin-2 associated
461 with PABP in translational repression. First, when Ataxin-2 target mRNAs are not actively
462 translated, then the mRNP through Me31B/DDX6 and PABP may recruit deadenylases to
463 transition into either a translationally dormant or degradative state (Lee *et al.*, 2017; Machida
464 *et al.*, 2018; Yi *et al*, 2018; Yoshida *et al.*, 2006). Second, Atx2 associated mRNA may move
465 into mRNP granules whose formation is facilitated by Atx2 IDR-mediated condensation. We
466 postulate that mRNAs in such assemblies are stored in a form that is protected from
467 degradation. While the above model, shown in Figure 6, is consistent with all our data, we

bioRxiv preprint doi: https://doi.org/10.1101/2022.02.15.480566; this version posted February 17, 2022. The copyright holder for this preprint (which was not certified by peer review) is the author/funder, who has granted bioRxiv a license to display the preprint in perpetuity. It is made available under aCC-BY-NC-ND 4.0 International license.

468 acknowledge that it needs extensive and rigorous testing in the context of the life cycle of a
469 single Ataxin-2 target mRNA.
470
471 **Implications for Ataxin-2 as a therapeutic target**
472 Antisense Oligonucleotide (ASO) based therapeutic strategies that lower levels of Atxn-2 are
473 being developed for the treatment of ALS and spinocerebellar ataxia type 2 (SCA2) (Becker *et*
474 *al.*, 2017; Scoles *et al.*, 2017). Our experiments provide a much finer grained analysis of
475 activities of Ataxin-2, suggesting that the function of the LSm domain should be spared, and
476 that IDR mediated assembly mechanisms and perhaps PAM2:PABP interactions should be
477 most usefully targeted by therapeutics.
478
479 Our previous work showed that *Atx2* mutants lacking the cIDR required for Ataxin-2 granule
480 formation in Drosophila neurons and S2 cells, were resistant to neurodegeneration as assessed
481 in *Drosophila* disease models (Bakthavachalu *et al.*, 2018; Huelsmeier *et al.*, 2021). We further
482 showed that the LSm-domain antagonizes Ataxin-2 granule formation (Singh et al, 2021). Here
483 we advance the latter observation by demonstrating that Ataxin-2 forms lacking the LSm
484 domain may more effectively cause cytotoxicity than the wild-type or IDR-deficient forms
485 (Figure 5C). These observations independently confirm our original conclusions and-provide
486 further support for a model in which the efficiency of mRNP assembly correlates with the speed
487 and severity of neurodegenerative processes in *Drosophila*.
488
489 The importance of the PAM2 domain in promoting degeneration has been previously observed
490 by experiments showing that heterologous expression of a pathogenic form of human Ataxin-
491 2 lacking its PAM2 domain, but not the full-length form, suppresses cytotoxicity in *Drosophila*
492 expressing human TDP-43 (Kim *et al.*, 2014). Our observations that expression of
493 Atx2ΔPAM2 is far less toxic than expression of wild-type Atx2 is consistent with this. In
494 addition, by showing that Atx2ΔPAM2 forms compositionally different Ataxin-2 granules,
495 they highlight the importance of specific granule components, and not granules *per se,* in
496 neurodegenerative pathologies. Thus, while liquid-liquid transitions mediated by disordered
497 domains could be a shared requirement for the formation of multiple types of mRNP granules,
498 we speculate that each granule type, with distinctive composition, could preferentially support
499 one or other type of proteinopathy (De Graeve & Besse, 2018; Vogler *et al*, 2018).
500
501 **Structured interactions may determine mRNP granule composition**.

bioRxiv preprint doi: https://doi.org/10.1101/2022.02.15.480566; this version posted February 17, 2022. The copyright holder for this preprint (which was not certified by peer review) is the author/funder, who has granted bioRxiv a license to display the preprint in perpetuity. It is made available under aCC-BY-NC-ND 4.0 International license.

502 Many lines of evidence argue that specific molecular interactions, e.g. mediated by structured
503 domains of the P-body component Edc3 or the stress-granule components G3BP and Caprin,
504 contribute to the mRNP granule formation (Decker *et al.*, 2007; Kedersha *et al*, 2016). In
505 engineered systems, the condensation of RNA-binding proteins and mRNAs into granules has
506 been clearly shown to depend on both traditional protein-protein interactions and on more
507 promiscuous interactions between intrinsically disordered regions (Protter *et al*, 2018). Our
508 work now identifies the interactions between Ataxin-2's PAM2 motif and PABP as a critical
509 contributor to the assembly of Ataxin-2 containing mRNP granules. This suggests a mechanism
510 by which the interaction helps select mRNA and protein components of mRNP granules.
511
512 We suggest that Ataxin-2, guided by PAM2:PABP interactions and LSm domain interactions,
513 recruits target mRNAs and associated proteins into translating mRNPs (Satterfield & Pallanck,
514 2006). Under conditions where the translation is arrested, LSm-domain interactions are altered
515 (Lee *et al.*, 2017), and transcripts are released from stalled ribosomes. Base-pairing interactions
516 between exposed mRNA side chains, as well as interactions between Ataxin-2's now
517 accessible intrinsically disordered regions, contribute to the assembly of these mRNPs into
518 granules. This logical sequence of events is consistent with: (a) TRIBE data showing a reduced
519 number of edits of native Ataxin-2 target mRNAs by Atx2ΔPAM2-ADARcd; (b) the inability
520 of ΔPAM2-miniAtx2 constructs to associate with stress granules; and (c) the aberrant protein
521 composition of granules induced by Atx2ΔPAM2 in S2 cells. The additional observation that
522 Atx2ΔPAM2-ADARcd expression results in a large number of non-native mRNA edits,
523 indicates that the PAM2:PABP interaction not only selects correct target mRNAs but also
524 prevents Ataxin-2 engagement with incorrect mRNA target regions.
525
526 Our conclusion that Ataxin2-PAM2:PABP interactions are involved in the selection of mRNA
527 components of RNP granules is superficially inconsistent with the observation that RNA
528 components of native stress granules can be predicted with remarkable accuracy on the basis
529 of mRNA size. This argues for a primary role for RNA-RNA interactions in the stress granule
530 assembly (Jain & Vale, 2017; Matheny *et al.*, 2021; Van Treeck & Parker, 2018). However,
531 we note that experiments presented here do not address mechanisms by which mRNAs are
532 selected into stress granules. Instead, the TRIBE data address how Atx2-target mRNAs are
533 selected into neuronal mRNP granules that exist in non-stressed cells *in vivo*, and microscopic
534 studies analyse protein components of mRNP granules formed following Atx2 expression in
535 S2 cells. Our experiments and observations therefore point to fundamental differences in

bioRxiv preprint doi: https://doi.org/10.1101/2022.02.15.480566; this version posted February 17, 2022. The copyright holder for this preprint (which was not certified by peer review) is the author/funder, who has granted bioRxiv a license to display the preprint in perpetuity. It is made available under aCC-BY-NC-ND 4.0 International license.

536 mechanisms by which the assembly of neuronal granules, or granule types found in unstressed
537 cells, may differ from those involved in stress-granule assembly. The regulation and
538 composition of the former class could well rely extensively on specific protein-protein and
539 protein-mRNA interactions, which may be revealed by future analyses of mechanisms by
540 which such mRNP assemblies are formed *in vivo*.
541

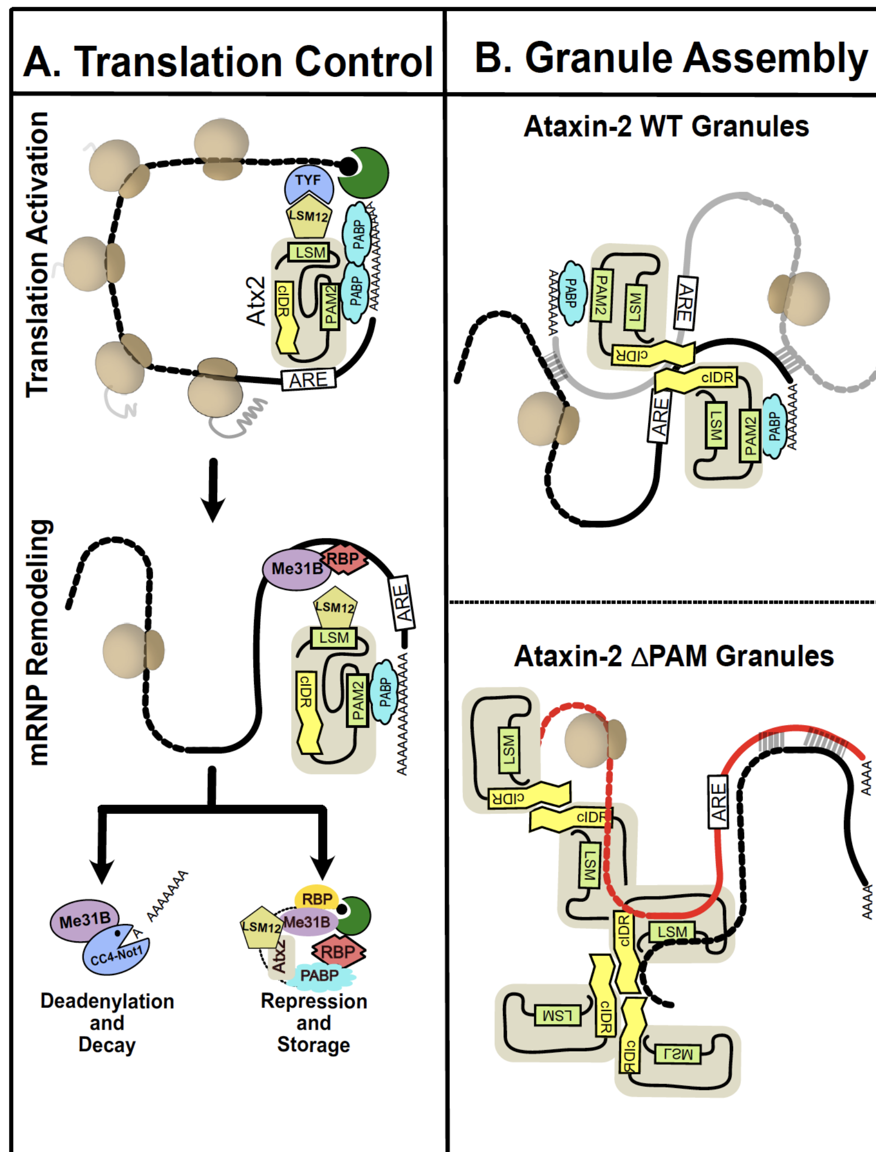

542
543
544 **Figure 6: A model for Ataxin-2 RNP dynamics and the role of PAM2 domain in determining its RNP**
545 **composition and mRNA selection.** (A) Ataxin-2 is recruited to mRNAs by RBPs during different stages
546 of the mRNA life cycle. Ataxin-2 activates translation of subsets of mRNA by recruiting LSM12, TYF and
547 other translation activation complexes. Under specific conditions, mRNP remodelling exposes Ataxin-2
548 cIDR that mediates multivalent interactions and RNP granule assembly. Ataxin-2 recruits Me31B and
549 CCR4-NOT1 complexes that lead to deadenylating and/or translation repression. It is possible that
550 LSM12/TYF continue to associate with RNA but are probably not part of repressor complexes. RNA

bioRxiv preprint doi: https://doi.org/10.1101/2022.02.15.480566; this version posted February 17, 2022. The copyright holder for this preprint (which was not certified by peer review) is the author/funder, who has granted bioRxiv a license to display the preprint in perpetuity. It is made available under aCC-BY-NC-ND 4.0 International license.

551 deadenylation can lead to degradation or translation repression and storage in RNP granules. (B) Ataxin-
552 2-PAM2 domain determines protein and RNA partners of the RNP granules. PAM2 domain is essential for
553 recruitment of Ataxin-2 to stress granules that also contains other RBPs (eg. Me31B, FMRP, Rox8, Rin
554 and Caprin). Ataxin-2-cIDR along with RNA-RNA interaction stabilise the stress induces RNP
555 condensation. In the absence of the PAM2 domain, Ataxin-2 fails to recruit specific target mRNA and
556 proteins. Remodelling of Ataxin-2 exposes the cIDR to induce phase separation and aberrant RNP
557 condensation. The Ataxin-2ΔPAM2 granules are non-toxic and lack several known stress granule proteins
558 (eg.FMRP, Caprin and PABP).
559

bioRxiv preprint doi: https://doi.org/10.1101/2022.02.15.480566; this version posted February 17, 2022. The copyright holder for this preprint (which was not certified by peer review) is the author/funder, who has granted bioRxiv a license to display the preprint in perpetuity. It is made available under aCC-BY-NC-ND 4.0 International license.

560 **Materials and methods**

561

562 Key resources table

563

Reagent type (species) or resource	Designation	Source or reference	Identifiers	Additional information
Genetic reagent (*Drosophila melanogaster*)	*UAS-Atx2-WT-ADARcd*	Singh *et al.* 2021	N/A	
Genetic reagent (*Drosophila melanogaster*)	*UAS-Atx2-ΔLSm-ADARcd*	Singh *et al.* 2021	N/A	
Genetic reagent (*Drosophila melanogaster*)	(*UAS-Atx2- ΔPAM2-ADARcd*)	This paper	N/A	
Genetic reagent (*Drosophila melanogaster*)	*UAS-Atx2- ΔcIDR-ADARcd*	Singh *et al.* 2021	N/A	
Genetic reagent (*Drosophila melanogaster*)	*UAS-Atx2-only LSm/Lsm-AD -ADARcd*	Singh *et al.* 2021	N/A	
Genetic reagent (*Drosophila melanogaster*)	*mef2-Gal4; Tub-Gal80^{ts}*	Bloomington *Drosophila* Stock center	Derived from #50742	
Genetic reagent (*Drosophila melanogaster*)	*elav-Gal4; Tub-Gal80^{ts}*	Bloomington *Drosophila* Stock center	Derived from #458	
Cell line (Drosophila melanogaster)	S2R+ cells	DGRC	RRID:CVCL_Z831	
Cell line (Human)	HEK293T	Gift: Adrian Bracken lab	N/A	
Cell line (Human)	U2OS	Gift: Martina Schroeder lab	N/A	
Recombinant DNA reagent	pUASt-Atx2-SNAP_fly (Plasmid)	This paper	N/A	Construct to express fly Atx2WT -SNAP
Recombinant DNA reagent	pUASt-ATXN2-SNAP_hum (Plasmid)	This paper	N/A	Construct to express human WT ATXN2-SNAP
Recombinant DNA reagent	pUASt-mini-Atx2-SNAP_fly (Plasmid)	This paper	N/A	Construct to express fly mini Atx2-SNAP
Recombinant DNA reagent	pUASt-mini-ATXN2-SNAP_hum (Plasmid)	This paper	N/A	Construct to express human mini ATXN2-SNAP
Recombinant DNA reagent	pUASt-ΔLSm-mini-Atx2-SNAP_fly (Plasmid)	This paper	N/A	Construct to express fly ΔLSm mini Atx2-SNAP
Recombinant DNA reagent	pUASt-ΔLSm-mini-ATXN2-SNAP_hum (Plasmid)	This paper	N/A	Construct to express human ΔLSm mini ATXN2-SNAP
Recombinant DNA reagent	pUASt-ΔLSmAD-mini-Atx2-SNAP_fly (Plasmid)	This paper	N/A	Construct to express fly ΔLSm-AD mini Atx2-SNAP
Recombinant DNA reagent	pUASt-ΔLSmAD-mini-ATXN2-SNAP_hum (Plasmid)	This paper	N/A	Construct to express human ΔLSm-AD mini ATXN2-SNAP
Recombinant DNA reagent	pUASt-ΔPAM2-mini-Atx2-SNAP_fly (Plasmid)	This paper	N/A	Construct to express fly ΔPAM2 mini Atx2-SNAP
Recombinant DNA reagent	pUASt-ΔPAM2-mini-ATXN2-SNAP_hum (Plasmid)	This paper	N/A	Construct to express human ΔPAM2 mini ATXN2-SNAP

bioRxiv preprint doi: https://doi.org/10.1101/2022.02.15.480566; this version posted February 17, 2022. The copyright holder for this preprint (which was not certified by peer review) is the author/funder, who has granted bioRxiv a license to display the preprint in perpetuity. It is made available under aCC-BY-NC-ND 4.0 International license.

Recombinant DNA reagent	pUASt-L859A-mini-Atx2-SNAP_fly (Plasmid)	This paper	N/A	Construct to express fly PAM2* L859A mini Atx2-SNAP
Recombinant DNA reagent	pUASt-L914A-mini-ATXN2-SNAP_hum (Plasmid)	This paper	N/A	Construct to express human PAM2* L914A mini ATXN2-SNAP
Recombinant DNA reagent	pUASt-F866A-mini-Atx2-SNAP_fly (Plasmid)	This paper	N/A	Construct to express fly PAM2* F866A mini Atx2-SNAP
Recombinant DNA reagent	pUASt-F921A-mini-ATXN2-SNAP_hum (Plasmid)	This paper	N/A	Construct to express human PAM2* F921A mini ATXN2-SNAP
Recombinant DNA reagent	pUASt-L859A-F866A-mini-Atx2-SNAP_fly (Plasmid)	This paper	N/A	Construct to express fly PAM2* L859A and F866A mini Atx2-SNAP
Recombinant DNA reagent	pUASt-L914A-F921A-Q928A-mini-ATXN2-SNAP_hum (Plasmid)	This paper	N/A	Construct to express human PAM2* L914A, F921A and Q928A mini ATXN2-SNAP
Recombinant DNA reagent	pAcman-Atx2-GFP (Fosmid)	Sudhakaran et al. 2013	N/A	Genomic construct to express fly WT Atx2-GFP
Recombinant DNA reagent	pAcman-ΔLSm-Atx2-GFP (Fosmid)	This paper	N/A	Genomic construct to express fly ΔLSm Atx2-GFP
Recombinant DNA reagent	pAcman-ΔPAM2-Atx2-GFP (Fosmid)	This paper	N/A	Genomic construct to express fly ΔPAM2 Atx2-GFP
Recombinant DNA reagent	pActin-Gal4	DGRC		Actin promoter Gal4 for insect UAS expression
Recombinant DNA reagent	pCMV-Gal4	Addgene	#24345	CMV promoter Gal4 for mammalian UAS expression
Antibody	Anti-Atx2 (chicken polyclonal)	Bakthavachalu et al., 2018	N/A	IF (1:1000) WB (1:1000)
Antibody	Anti-Caprin (rabbit polyclonal)	Papoulas et al., 2010	N/A	IF (1:1000)
Antibody	Anti-dFMR (mouse monoclonal)	DSHB	# 5A11	IF (1:1000) deposited to the DSHB by Siomi, H.
Antibody	Anti-GFP (chicken polyclonal)	Abcam	Cat# mAb 13970	IF (1:1000)
Antibody	Anti-V5 (rabbit polyclonal)	Santa Cruz Biotechnology	Cat# sc83849-R	IF (1:1000) WB (1:1000)
Antibody	PABP (rabbit polyclonal serum)	Lee et al. 2017	N/A	IF (1:500) WB (1:500)
Antibody	Me31B (rabbit polyclonal serum)	Lee et al. 2018	N/A	IF (1:500)
Antibody	Rox8 (rat polyclonal)	Buddika et al. 2020	N/A	IF (1:1000)
Antibody	SNAP (rabbit polyclonal)	NEB	Cat# P9310S	WB (1:1000)
Antibody	PABPC1 (rabbit polyclonal)	Abcam	Cat# ab21060	WB (1:1000)
Antibody	LSM12 (rabbit anti human polyclonal)	Abcam	Cat# ab173292	WB (1:1000)
Antibody	G3BP (mouse monoclonal)	BD Bioscience	Cat# 611126	IF (1:1000)
Antibody	Histone H3 (rabbit polyclonal)	Cell signaling tech	Cat# 9715	WB (1:1000)
Antibody	Baf155 (rabbit monoclonal)	Cell signaling tech	Cat# 11956	WB (1:1000)

bioRxiv preprint doi: https://doi.org/10.1101/2022.02.15.480566; this version posted February 17, 2022. The copyright holder for this preprint (which was not certified by peer review) is the author/funder, who has granted bioRxiv a license to display the preprint in perpetuity. It is made available under aCC-BY-NC-ND 4.0 International license.

Antibody	HRP Goat anti-rabbit	Invitrogen	Cat# A16104	WB (1:10,000)
Antibody	HRP Goat anti-mouse	Invitrogen	Cat# 31430	WB (1:10,000)
Antibody	Alexa Fluor 555 (polyclonal goat anti-chicken IgG)	Invitrogen	Cat# A21437	IF (1:1000)
Antibody	Alexa Fluor 488 (polyclonal goat anti-chicken IgG)	Invitrogen	Cat# A11039	IF (1:1000)
Antibody	Alexa Fluor 647 (polyclonal goat anti-chicken IgG)	Invitrogen	Cat# A21449	IF (1:1000)
Antibody	Alexa Fluor 555 (polyclonal goat anti-rabbit IgG)	Invitrogen	Cat# A21428	IF (1:1000)
Antibody	Alexa Fluor 488 (polyclonal goat anti-rabbit IgG)	Invitrogen	Cat# A11078	IF (1:1000)
Antibody	Alexa Fluor 647 (polyclonal goat anti-rabbit IgG)	Invitrogen	Cat# A21244	IF (1:1000)
Antibody	Alexa Fluor 555 (polyclonal goat anti-mouse IgG)	Invitrogen	Cat# A21422	IF (1:1000)
Antibody	Alexa Fluor 488 (polyclonal goat anti-mouse IgG)	Invitrogen	Cat# A21121	IF (1:1000)
Antibody	Alexa Fluor 647 (polyclonal goat anti-mouse IgG)	Invitrogen	Cat# A21235	IF (1:1000)
Chemical compound	MOWIOL mounting medium	Sigma (Merck)	Cat# 81381	
Chemical compound	SNAP-TmrStar	New England Biolabs	Cat# S9105S	IF (1:1000)
Chemical compound	SNAP-Surface 488	New England Biolabs	Cat# S9124S	IF (1:1000)
Software, algorithm	TRIBE	McMahon et al., 2016	https://github.com/rosbashlab/TRIBE	
Software, algorithm	STAR v2.5.3	Dobin et al., 2013	https://github.com/alexdobin/STAR	
Software, algorithm	HTSeq v0.11.2	Anders et al., 2015	https://github.com/htseq/htseq	
Software, algorithm	DESeq2	Love et al., 2014	https://bioconductor.org/packages/release/bioc/html/DESeq2.html	
Software, algorithm	ARE*Score*	Spasic et al., 2012	http://arescore.dkfz.de/arescore.pl	
Software, algorithm	Guitar	Cui et al., 2016	https://bioconductor.org/packages/release/bioc/html/Guitar.html	
Software, algorithm	Bedtools	Quinlan and Hall, 2010	https://github.com/arq5x/bedtools2	
Software, algorithm	twoBitToFa	-	https://genome.ucsc.edu/goldenPath/help/twoBit.html	
Software, algorithm	MEME suite	Bailey et al., 2009	http://meme-suite.org/tools/meme	
Software, algorithm	ImageJ	Schneider et al., 2012	https://imagej.nih.gov/ij/	

bioRxiv preprint doi: https://doi.org/10.1101/2022.02.15.480566; this version posted February 17, 2022. The copyright holder for this preprint (which was not certified by peer review) is the author/funder, who has granted bioRxiv a license to display the preprint in perpetuity. It is made available under aCC-BY-NC-ND 4.0 International license.

Software, algorithm	Ggplot2	Wilkinson, 2011	https://github.com/tidyverse/ggplot2	
Software, algorithm	Pheatmap		https://cran.r-project.org/web/packages/pheatmap/index.html	
Software, algorithm	SnapDragon		https://www.flyrnai.org/snapdragon	

564

565 Cell culture, transfection and stress induction

566 *Drosophila* S2R+ cells were obtained from the DGRC, Indiana University, and were grown in
567 Gibco Schneider's S2 media with 10% FBS and 1% penicillin and streptomycin, at 25°C.
568 Transfections were performed using either FugeneHD (Active Motif) or TransIT-X2 (Mirus)
569 reagents at 2:1 ratio µl reagent to µg plasmid DNA for 24-72 h depending on downstream use.
570 HEK293T cells from Adrian Bracken, Trinity College Dublin, were grown in Gibco
571 Dulbecco's Modified Eagle Media with 10% FBS, 2 mM l-glutamine addition, 1% penicillin
572 and streptomycin, at 37°C and 5% CO2. U2OS cells from Martina Schroeder, Maynooth
573 University, were grown at the same conditions as HEK293T. Mammalian cell transfections
574 were carried out with 1 mM PEI (Polysciences) solution at 2:1 ratio µl reagent to µg plasmid
575 DNA for 24-72H depending on downstream use. For confocal imaging applications cells were
576 grown in 24-well plates on glass cover-slips for 24 h before transfection for up to 48 h. For
577 Western blotting and IP, cells were grown in 75 cm^2 flasks until >80% confluent before
578 transfection for up to 72H before harvesting. Oxidative stress was induced in *Drosophila* S2R+
579 cells with addition of sodium arsenite solution to a final concentration of 50 µM in media for
580 3 h. In mammalian cells, oxidative stress was induced in the same way except for only 1 h.

581

582 Western blotting and protein immunoprecipitation

583 Total protein extracts were prepared from S2 and HEK293 cells as described earlier
584 (Sudhakaran et al., 2014). Up to 10 µg total protein was loaded per well for detecting Atx2-
585 SNAP constructs, partner proteins and loading controls on 8-12% SDS-PAGE gels and
586 transferred to nitrocellulose membranes. The blots were probed in 5% skim milk in PBS using
587 rabbit anti-SNAP (1:1000), rabbit anti-PABP (1:1000), rabbit anti-LSM12 (1:1000) antibodies,
588 and mouse anti-histone H3 (1:5000) and mouse anti-BAF155 (1:2000) loading control
589 antibodies. Corresponding HRP-conjugated secondary antibodies were used at 1:10,000
590 dilution and developed using Pierce ECL western blotting substrate (ThermoFisher) as per the
591 manufacturer's instructions.

bioRxiv preprint doi: https://doi.org/10.1101/2022.02.15.480566; this version posted February 17, 2022. The copyright holder for this preprint (which was not certified by peer review) is the author/funder, who has granted bioRxiv a license to display the preprint in perpetuity. It is made available under aCC-BY-NC-ND 4.0 International license.

592 For Atx2-SNAP construct immunoprecipitation, transfected cell lysates were normalised to the
593 same volume and concentration, 10% of the volume was saved and diluted as an input control,
594 and Chromotek anti-SNAP-tag conjugated agarose beads and IP kits were used according to
595 the manufacturer's specifications. Pulled-down proteins together with corresponding sample
596 input controls were blotted as described above.
597
598 Immunohistochemistry and imaging of cultured cells
599 Transfected cells on coverslips were fixed with 4% paraformaldehyde in PBS solution for 15
600 min, followed by three 5 min washes in PBS. Permeabilization was performed on all cells with
601 0.5% TritonX100 in PBS solution for 3 min, before three more 5 min washes in PBS. Cells
602 were blocked with 3% BSA in PBS for 1 h at room temperature before staining with primary
603 antibodies at appropriate dilutions in 3% BSA overnight at 4°C. Corresponding fluorescent
604 secondary antibodies in 3% BSA were used to stain the sample cells for 1 h at room temperature
605 after primaries were washed off. Where SNAP-tagged proteins were being visualized, SNAP-
606 ligand TMR-Star (NEB) or SNAP-surface-Alexa488 (NEB) were added at the secondary
607 antibody staining stage. Following staining and washing, cells were mounted upside-down on
608 microscopy slides in MOWIOL, allowed to cure for >12 h at 4 °C, and imaged on a Zeiss
609 LSM880 Airyscan/AiryscanFast confocal microscope with a 20x air objective.
610
611 Bioimage analysis
612 Where relevant, Airyscan images were processed with Zen Black software (Zeiss) with
613 recommended settings. Confocal microscopy images were analysed using macros within
614 ImageJ/FIJI and Excel. Quantification of co-localisation was performed by comparing stress
615 granule marker staining intensity profiles across a randomised selection of Atx2 granules
616 within transfected cells, with the intensity profile of the Atx2 staining. Any signal 10% or
617 higher than background (adjusted for fluorophore bleed through) was deemed evidence of co-
618 localisation within that particular granule. For quantifying the exclusion of mini-Atx2-SNAP
619 constructs from stress induced granules the Caprin or G3BP1 staining was used as independent
620 identifier of stress granules and Atx2 profiles were compared to them. 48-120 granules were
621 quantified in each co-staining (Figure 2), and 28-70 granules were quantified for each construct
622 transfection (Figure 4).
623
624 Crystal structure threading

bioRxiv preprint doi: https://doi.org/10.1101/2022.02.15.480566; this version posted February 17, 2022. The copyright holder for this preprint (which was not certified by peer review) is the author/funder, who has granted bioRxiv a license to display the preprint in perpetuity. It is made available under aCC-BY-NC-ND 4.0 International license.

625 Threading of the *Drosophila* PAM2 peptide bound to the MLLE domain of PABPC1 was
626 performed using the Swiss-PdbViewer software, based on the human crystal structure of the
627 complex obtained from PDB, identified as 3KTR (Kozlov et al., 2010)
628
629 Experimental fly crosses
630 *Drosophila* stocks were maintained at 25°C in corn meal agar. Strains homozygous for UAS-
631 transgenes were crossed with *elav-Gal4* and *tub-Gal80ts* at 18 °C till the adult fly emerged.
632 The flies were shifted to 29 °C for 5 days before processing for RNA extraction for TRIBE
633 experiments. The climbing behaviour experiments were performed on flies kept at 29 °C for
634 either 1 or 15 days. For microCT experiments, the UAS-transgenes were crossed with *mef2-*
635 *Gal4* and *tub-Gal80ts* at 18°C and the adult flies were transferred to 29 °C for 1 day or 20 days.
636
637 RNA extraction from brain and NGS
638 Around 10-12 adult brains were dissected in RNA Later for total RNA isolation. RNA was
639 isolated using TRIzol reagent (Invitrogen) as per the manufacturer's protocol. Poly(A)-
640 enriched mRNA was used to prepare Illumina libraries using the NEBNext Ultra II Directional
641 RNA Library Prep kit (E7765L). Atx2-ΔPAM2-ADARcd samples were sequenced with
642 Illumina HiSeq PE Rapid Cluster Kit v2 (PE-402-4002) to generate 2 × 100 paired-end strand-
643 specific data using the Illumina HiSeq 2500 sequencing platform.
644
645 TRIBE data analysis
646 The sequencing reads obtained had a mean quality score (Q-Score) >= 37. Analysis of the
647 TRIBE data was performed as described previously (McMahon et al., 2016, Singh et al., 2021).
648 Briefly, the reference genome and gtf file of *Drosophila melanogaster*, version dm6, were
649 downloaded from the UCSC genome browser. Raw sequencing reads were mapped using
650 TopHat2 (Trapnell *et al*, 2009) with the parameters '--library-type fr-firststrand -m 1 N 3 --
651 read-edit-dist 3 p 5 g 2 -I 50000 --microexon-search --no-coverage-search -G dm6_genes.gtf'.
652 Only uniquely mapped reads are considered for editing analysis. A table of raw and mapped
653 reads is included in Supplementary Table 1. A threshold file was created by ensuring only edits
654 with coverage of at least 20 reads and 15% edits were retained. All the TRIBE experiments
655 were performed in duplicates, and only the edits identified in both replicates above the edit
656 threshold are reported.
657 Climbing Assay:

bioRxiv preprint doi: https://doi.org/10.1101/2022.02.15.480566; this version posted February 17, 2022. The copyright holder for this preprint (which was not certified by peer review) is the author/funder, who has granted bioRxiv a license to display the preprint in perpetuity. It is made available under aCC-BY-NC-ND 4.0 International license.

658 Appropriately aged adult *Drosophila* was transferred to a 50 ml graduated glass measuring
659 cylinder for the climbing assay and sealed with a cotton plug. A digital video camera was
660 positioned to record the vials. The assay was initiated by tapping the cylinder against a foam
661 pad to collect the flies to the bottom of the cylinder and the flies were allowed to climb the
662 cylinder with video being recorded for ~30 s. The number of flies that crossed the 20 ml mark
663 (~5.5cm) was counted over time and the data was plotted against the time using GraphPad
664 prism. Average of 3 trials were used for each biological replicate. 7-10 biological replicates
665 were used for each genotype.
666
667 Sample preparation and scanning for microCT**:**
668 *Drosophila* indirect flight muscle microCT was carried out as described in Chaturvedi et. al,
669 2019. Briefly, animals were anesthetized on ice and fixed in PBS containing 4%
670 paraformaldehyde (PFA). Thoraces were dissected and stained using 1% elemental iodine
671 (1.93900.0121, Emparta, Merck) with 2% potassium iodide (no. 15 724, Qualigens) dissolved
672 in PBS. The stained samples were washed in PBS and embedded in petroleum jelly. MicroCT
673 scanning was carried out at 40 kV, 250 µA, on Bruker Skyscan-1272.
674
675 Data availability
676 The RNA sequencing data have been deposited to GEO under the accession code
677 GSE196739.
678
679 Contact for reagent and resource sharing
680 Further information and requests for resources and reagents should be directed to and will be
681 fulfilled by the lead contacts Mani Ramaswami (mani.ramaswami@tcd.ie) and Baskar
682 Bakthavachalu (baskar@iitmandi.ac.in).
683
684 **ACKNOWLEDGEMENTS:**
685
686 We thank members of the Ramaswami, Vijay Raghavan and Bakthavachalu labs and Roy
687 Parker for useful discussions and/or comments on the manuscript. We thank Marlena Mucha,
688 Adrian Bracken and Amir Khan for advice and help with biochemical experiments, Michael
689 Rosbash for *Drosophila* TRIBE plasmids, and colleagues acknowledged in the Key Resources
690 table for reagents and advice. The fly facility at Bangalore Life Science Cluster (BLiSC)

bioRxiv preprint doi: https://doi.org/10.1101/2022.02.15.480566; this version posted February 17, 2022. The copyright holder for this preprint (which was not certified by peer review) is the author/funder, who has granted bioRxiv a license to display the preprint in perpetuity. It is made available under aCC-BY-NC-ND 4.0 International license.

691 provided support with fly stock supply as well as generation of transgenic; CIFF at BLiSC
692 provided essential confocal microscopy support; and Awadhesh Pandit and next-generation
693 genomics facility at BLiSC provided NGS service. Daniel Fortunati thanks Kenneth Mok for
694 his mentorship. We acknowledge Drosophila Genomics Resource Centre (supported by NIH
695 grant 2P40OC010949) for *Drosophila* S2 cells.
696

697 **FUNDING:**

698 The work was supported by a Science Foundation Ireland (SFI) Investigator grant to MR and
699 NCBS-TIFR intramural funding to KVR. BB is supported by the DBT/Wellcome Trust India
700 Alliance Fellowship (IA/I/19/1/504286). We acknowledge the support from an Irish Research
701 Council Postgraduate Fellowship to DF, the J. C. Bose Fellowship of the Government of India
702 (KVR), INSA Young Scientist Project (INSA/SP/YSP/143/2017) (AS), SERB to MR from a
703 collaborative VAJRA award to Dr. Raghu Padinjat, and a DST INSPIRE fellowship (KA). We
704 thank C-CAMP for logistical support for SSP.
705

706 **AUTHOR CONTRIBUTIONS:**

707 Conceptualization, A.P., D.F, A.S., J.Huelsmeier, K.V.R., M.R., and B.B.; Methodology, A.P.,
708 D.F, A.S., J.Huelsmeier, A.R.K., S.S.P., J.Hillebrand, K.A., D.J., G.B., J.L., C.L., G.A.,
709 K.H.M., K.V.R., M.R., and B.B.; Investigation, A.S., J.Huelsmeier, A.R.K., S.S.P.,
710 J.Hillebrand, A.P., K.A., K.V.R., M.R., and B.B.; Writing–Original Draft, A.P., D.F, A.S.,
711 J.Huelsmeier, K.V.R., M.R., and B.B.; Writing–Review & Editing, A.P., D.F, A.S.,
712 J.Huelsmeier, A.R.K., S.S.P., J.Hillebrand, K.A., D.J., G.B., J.L., C.L., G.A., K.H.M., K.V.R.,
713 M.R., and B.B.; Funding Acquisition, K.V.R., M.R., and B.B.; Resources, Fly community.
714

715 **DECLARATION OF INTERESTS:** The authors declare no conflicts of interest.
716
717
718

bioRxiv preprint doi: https://doi.org/10.1101/2022.02.15.480566; this version posted February 17, 2022. The copyright holder for this preprint (which was not certified by peer review) is the author/funder, who has granted bioRxiv a license to display the preprint in perpetuity. It is made available under aCC-BY-NC-ND 4.0 International license.

719 **SUPPLEMENTARY FIGURES:**

720 **Supplementary Figure 1:**

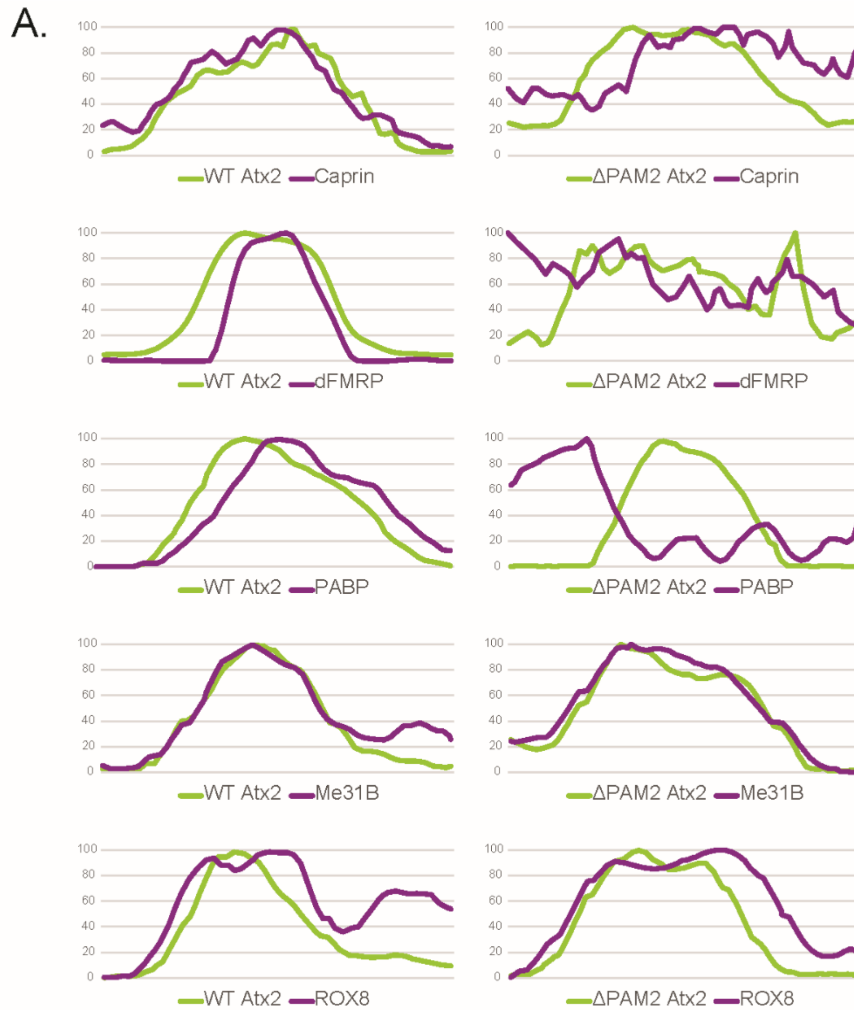

B.

Co-localisation of signal enrichment in granules		
	WT Atx2	ΔPAM2 Atx2
Caprin	100.0%	7.1%
dFMRP	100.0%	2.4%
PABP	76.7%	14.6%
Me31B	66.7%	52.0%
Rox8	100%	100%

C.

	Drosophila Mini Atx2-SNAP Version						
Construct	WT	ΔLSm	ΔLSm-AD	ΔPAM2	L859A	F866A	Double*
% enrichment in SGs	88.60%	80.00%	93.30%	4.60%	0.00%	0.00%	0.00%

	Human Mini Atxn2-SNAP Version						
Construct	WT	ΔLSm	ΔLSm-AD	ΔPAM2	L914A	F921A	Triple*
% enrichment in SGs	100.00%	96.20%	100.00%	4.90%	0.00%	5.00%	4.80%

721

722 **Supplementary Figure 1:** Co-localisation quantification for figure 2, figure 4. (A) Normalised
723 profile plots of Atx2-GFP granules in S2 cells as shown in Figure 2. Within representative
724 granules of wild type Atx2-GFP (green line), SG components Caprin, dFMRP, PABP, Me31B,
725 and Rox8 show largely overlapping enrichment of fluorescence profile along a line bisecting a
726 granule after immunohistochemistry and imaging (purple line). In Atx2ΔPAM2-GFP granules,

bioRxiv preprint doi: https://doi.org/10.1101/2022.02.15.480566; this version posted February 17, 2022. The copyright holder for this preprint (which was not certified by peer review) is the author/funder, who has granted bioRxiv a license to display the preprint in perpetuity. It is made available under aCC-BY-NC-ND 4.0 International license.

727 this colocalization of fluorescence signals is not seen in the case of Caprin, dFMRP and PABP,
728 suggesting these components are not enriched in these granules above background level. (B)
729 Quantification of co-localization for Figure 2. N = 48-120 images of Atx2-GFP granules were
730 randomly selected for each co-staining and analysed for signal co-enrichment (see methods) in
731 the case of each component assayed. (C) Quantification of Atx2 construct inclusion in SGs for
732 Figure 4. N = 28-70 images of stress granules in arsenite stressed S2 cells (marked by anti-
733 Caprin staining) and U2OS cells (marked by anti-G3BP staining) were randomly selected for
734 each Atx2 construct assayed and were analysed for Mini Atx2-SNAP allele signal co-
735 enrichment (see methods).
736

bioRxiv preprint doi: https://doi.org/10.1101/2022.02.15.480566; this version posted February 17, 2022. The copyright holder for this preprint (which was not certified by peer review) is the author/funder, who has granted bioRxiv a license to display the preprint in perpetuity. It is made available under aCC-BY-NC-ND 4.0 International license.

737 **Supplementary Figure 2:**

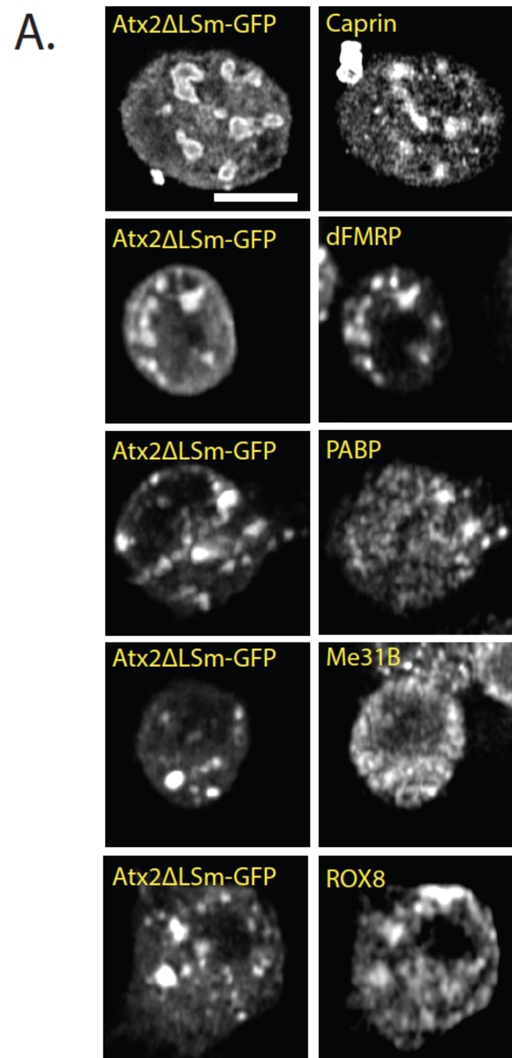

738

739 **Supplementary Figure 2:** Atx2ΔLSm granules in S2 cells do not show significantly altered
740 protein contents compared to wild-type Atx2. Caprin, dFMRP, PABP, Me31B, and Rox8 co-
741 localize with overexpressed Atx2ΔLSm GFP, suggesting that the granules formed contain a
742 similar set of components as Atx2 granules. It should be noted that Atx2 granules do not
743 sequester the majority of the endogenous components stained for, leading to a high, diffuse
744 background staining.

745

bioRxiv preprint doi: https://doi.org/10.1101/2022.02.15.480566; this version posted February 17, 2022. The copyright holder for this preprint (which was not certified by peer review) is the author/funder, who has granted bioRxiv a license to display the preprint in perpetuity. It is made available under aCC-BY-NC-ND 4.0 International license.

746 **Supplementary Figure 3:**

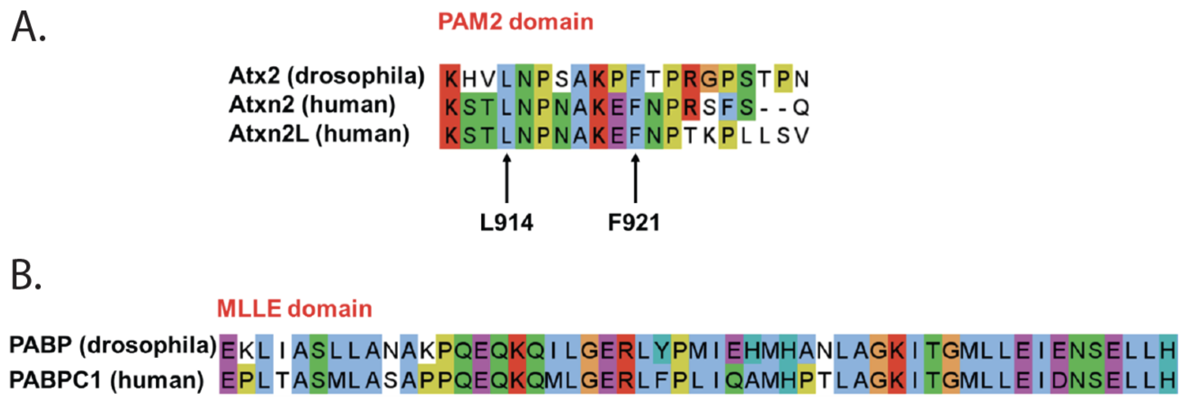

747

748

749 **Supplementary Figure 3:** The ATXN2 PAM2 and the PABPC1 MLLE domain are highly
750 conserved from fly to human. (A) The ATXN2 PAM2 domain exhibits high sequence
751 similarity where the key MLLE domain hydrophobic binding residues leucine 914 and
752 phenylalanine 921 (human ATXN2 numbering) are conserved from *Drosophila* to humans. (B)
753 Its binding partner, the PABPC1 MLLE domain, is also highly conserved from *Drosophila* to
754 human. Sequence IDs: Q8SWR8 (Atx2_DROME), Q99700 (ATXN2_HUMAN), Q8WWM7
755 (ATX2L_HUMAN), P21187 (PABP_DROME), P11940 (PABP1_HUMAN).

756

757

bioRxiv preprint doi: https://doi.org/10.1101/2022.02.15.480566; this version posted February 17, 2022. The copyright holder for this preprint (which was not certified by peer review) is the author/funder, who has granted bioRxiv a license to display the preprint in perpetuity. It is made available under aCC-BY-NC-ND 4.0 International license.

758 **Supplementary Figure 4:**

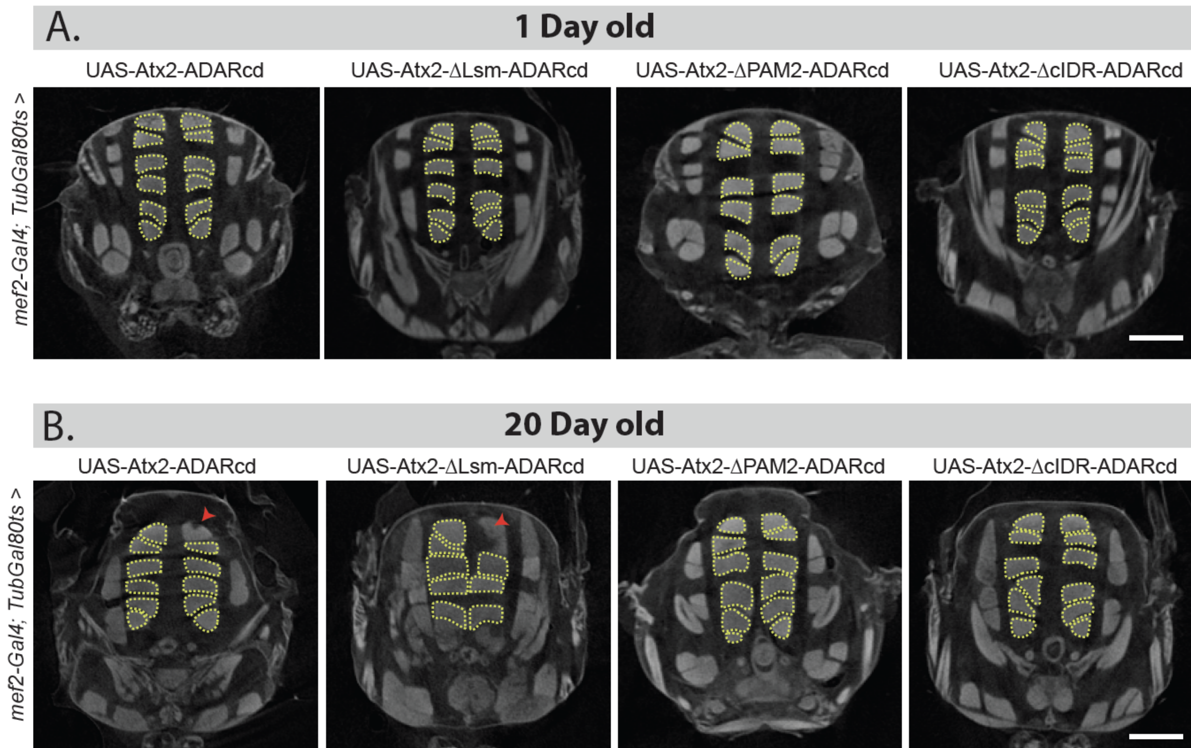

759

760 **Supplementary Figure 4:** Transverse view of *Drosophila* indirect flight muscle imaged using
761 micro-CT show cellular toxicity. (A) Driving UAS-transgene (Atx2WT, Atx2ΔcIDR,
762 Atx2ΔPAM or Atx2ΔLSm) with *mef2-Gal4* show normal muscles on day 1. (B) Expression of
763 wild-type and Atx2ΔLSm transgene for 20 days show loss of muscle fibers, indicated with
764 solid red arrowheads. Expression of Atx2ΔPAM2 and Atx2ΔcIDR for 20 days show no visible
765 phenotype.

766

bioRxiv preprint doi: https://doi.org/10.1101/2022.02.15.480566; this version posted February 17, 2022. The copyright holder for this preprint (which was not certified by peer review) is the author/funder, who has granted bioRxiv a license to display the preprint in perpetuity. It is made available under aCC-BY-NC-ND 4.0 International license.

767 **Supplementary Table 1:**
768

S.NO	Sample Name	Million reads (Paired end)		Total Number of Million reads	% >= Q30	Mean Quality Score	Mapping Percentage Read 1	Mapping Percentage Read 2
		Read 1	Read 2					
1	Atx2ΔPAM2-ADARcd rep_1	23.75	23.75	47	97.04	38.26	92.20%	92.10%
2	Atx2ΔPAM2-ADARcd rep_2	22.66	22.66	45	97.03	38.26	91.30%	91.20%

769
770
771 **Supplementary Table 2:** The targets common between Atx2 wild-type and del-PAM2 are
772 shown in bold text.
773

Chr	Start	End	Genes	Replicate 1 edit percentage	Replicate 2 edit percentage	Average edit percentage	Chr_coordinate
chr2L	**1009080**	**1009081**	**IA-2**	**17.1**	**15.5**	**16.3**	**chr2L_1009081_IA-2**
chr2L	**1009440**	**1009441**	**IA-2**	**31.7**	**38.8**	**35.25**	**chr2L_1009441_IA-2**
chr2L	**1011482**	**1011483**	**IA-2**	**31.7**	**34.7**	**33.2**	**chr2L_1011483_IA-2**
chr2L	13505104	13505105	B4	22.4	17.48	19.94	chr2L_13505105_B4
chr2L	**17188307**	**17188308**	**beat-IIIc**	**18**	**21.7**	**19.85**	**chr2L_17188308_beat-IIIc**
chr2L	19746161	19746162	CG10631	25.65	19.4	22.52	chr2L_19746162_CG10631
chr2L	**20056018**	**20056019**	**sNPF**	**16**	**24.3**	**20.15**	**chr2L_20056019_sNPF**
chr2L	7891375	7891376	Snoo	18.5	16.7	17.6	chr2L_7891376_Snoo
chr2L	8113160	8113161	Bsg	17.4	19.05	18.23	chr2L_8113161_Bsg
chr2L	**8113894**	**8113895**	**Bsg**	**16.82**	**28.7**	**22.76**	**chr2L_8113895_Bsg**
chr2L	8116005	8116006	Bsg	18.2	27.4	22.8	chr2L_8116006_Bsg
chr2L	9256901	9256902	Ggamma30A	19.5	32.6	26.05	chr2L_9256902_Ggamma30A
chr2L	**9292530**	**9292531**	**Ggamma30A**	**42**	**54.4**	**48.2**	**chr2L_9292531_Ggamma30A**
chr2L	**9292829**	**9292830**	**Ggamma30A**	**42.6**	**53.55**	**48.08**	**chr2L_9292830_Ggamma30A**
chr2L	9295031	9295032	Ggamma30A	23.5	26	24.75	chr2L_9295032_Ggamma30A
chr2R	12085463	12085464	jeb	16	28.4	22.2	chr2R_12085464_jeb
chr2R	**13513577**	**13513578**	**Vmat**	**64.2**	**63.9**	**64.05**	**chr2R_13513578_Vmat**
chr2R	13513654	13513655	Vmat	27.7	33.45	30.58	chr2R_13513655_Vmat
chr2R	**13513732**	**13513733**	**Vmat**	**24**	**29.75**	**26.88**	**chr2R_13513733_Vmat**
chr2R	**13513762**	**13513763**	**Vmat**	**44.55**	**47.3**	**45.92**	**chr2R_13513763_Vmat**
chr2R	**13514350**	**13514351**	**Vmat**	**37.7**	**38.5**	**38.1**	**chr2R_13514351_Vmat**
chr2R	13519080	13519081	Vmat	18.1	20.8	19.45	chr2R_13519081_Vmat
chr2R	**23690701**	**23690702**	**Pal2**	**17.3**	**17.2**	**17.25**	**chr2R_23690702_Pal2**
chr2R	24213943	24213944	CG30419	27.8	22.98	25.39	chr2R_24213944_CG30419
chr2R	24214234	24214235	CG30419	24.2	26.1	25.15	chr2R_24214235_CG30419
chr2R	24214648	24214649	CG30419	16.4	15.9	16.15	chr2R_24214649_CG30419
chr2R	24215193	24215194	CG30419	43.5	29.7	36.6	chr2R_24215194_CG30419
chr2R	24229341	24229342	CG30419	20.8	16.3	18.55	chr2R_24229342_CG30419
chr2R	6914804	6914805	CG30158	16.4	16	16.2	chr2R_6914805_CG30158
chr2R	**6920815**	**6920816**	**CG30158**	**33.92**	**40.48**	**37.2**	**chr2R_6920816_CG30158**
chr2R	**6921435**	**6921436**	**CG30158**	**17.5**	**41.9**	**29.7**	**chr2R_6921436_CG30158**
chr2R	**6921976**	**6921977**	**CG30158**	**36**	**40.2**	**38.1**	**chr2R_6921977_CG30158**
chr2R	**7718070**	**7718071**	**CG18812**	**15.9**	**19.7**	**17.8**	**chr2R_7718071_CG18812**

bioRxiv preprint doi: https://doi.org/10.1101/2022.02.15.480566; this version posted February 17, 2022. The copyright holder for this preprint (which was not certified by peer review) is the author/funder, who has granted bioRxiv a license to display the preprint in perpetuity. It is made available under aCC-BY-NC-ND 4.0 International license.

chr2R	9473772	9473773	Camta	21.75	30.18	25.96	chr2R_9473773_Camta
chr2R	9479421	9479422	Camta	23.1	26	24.55	chr2R_9479422_Camta
chr2R	**9480019**	**9480020**	**Camta**	**32**	**41**	**36.5**	**chr2R_9480020_Camta**
chr2R	**9910328**	**9910329**	**FMRFa**	**42.5**	**25**	**33.75**	**chr2R_9910329_FMRFa**
chr3L	**11498209**	**11498210**	**chrb**	**15.82**	**20.5**	**18.16**	**chr3L_11498210_chrb**
chr3L	12267895	12267896	CG32100	20	16.1	18.05	chr3L_12267896_CG32100
chr3L	1504295	1504296	Psa	18.6	15.9	17.25	chr3L_1504296_Psa
chr3L	1521650	1521651	Psa	18.5	34.6	26.55	chr3L_1521651_Psa
chr3L	1543675	1543676	CG7852	15.5	22	18.75	chr3L_1543676_CG7852
chr3L	17062355	17062356	Rbp6	15.2	18.5	16.85	chr3L_17062356_Rbp6
chr3L	17147382	17147383	Rbp6	18.23	26.62	22.42	chr3L_17147383_Rbp6
chr3L	**17345219**	**17345220**	**Mip**	**29.9**	**27.2**	**28.55**	**chr3L_17345220_Mip**
chr3L	**17345290**	**17345291**	**Mip**	**17.9**	**16.9**	**17.4**	**chr3L_17345291_Mip**
chr3L	**19066983**	**19066984**	**Mkp3**	**18.9**	**15.7**	**17.3**	**chr3L_19066984_Mkp3**
chr3L	21494821	21494822	Hr78	27.1	18.4	22.75	chr3L_21494822_Hr78
chr3L	21831417	21831418	CG7148	15.8	28.6	22.2	chr3L_21831418_CG7148
chr3L	21930851	21930852	mub	15	17.2	16.1	chr3L_21930852_mub
chr3L	21931110	21931111	mub	15.1	20.1	17.6	chr3L_21931111_mub
chr3L	22061206	22061207	Oct-TyrR	15.4	16.7	16.05	chr3L_22061207_Oct-TyrR
chr3L	22877661	22877662	Chro	35.3	45.7	40.5	chr3L_22877662_Chro
chr3L	23148124	23148125	CG32350	27.4	35.3	31.35	chr3L_23148125_CG32350
chr3L	23747549	23747550	CG17698	40.27	28.95	34.61	chr3L_23747550_CG17698
chr3L	23934990	23934991	CG40470	23.5	22.05	22.77	chr3L_23934991_CG40470
chr3L	3910071	3910072	Eip63F-1	20	24.5	22.25	chr3L_3910072_Eip63F-1
chr3L	**3954338**	**3954339**	**CG12605**	**35.2**	**40.8**	**38**	**chr3L_3954339_CG12605**
chr3L	**3954933**	**3954934**	**CG12605**	**35.42**	**51.1**	**43.26**	**chr3L_3954934_CG12605**
chr3L	3957068	3957069	CG12605	21.8	26.7	24.25	chr3L_3957069_CG12605
chr3L	3957671	3957672	CG12605	18.9	22.2	20.55	chr3L_3957672_CG12605
chr3L	3961590	3961591	CG12605	18.3	18.5	18.4	chr3L_3961591_CG12605
chr3L	3992789	3992790	scrt	21.08	27.28	24.18	chr3L_3992790_scrt
chr3L	4092142	4092143	CG14989	15.88	18.6	17.24	chr3L_4092143_CG14989
chr3L	4113123	4113124	Ack	18.4	16.7	17.55	chr3L_4113124_Ack
chr3L	4113297	4113298	Ack	18.4	17.9	18.15	chr3L_4113298_Ack
chr3L	572527	572528	hipk	29.8	31	30.4	chr3L_572528_hipk
chr3L	572530	572531	hipk	42.7	43	42.85	chr3L_572531_hipk
chr3L	**575712**	**575713**	**hipk**	**36.12**	**52.92**	**44.52**	**chr3L_575713_hipk**
chr3L	**575753**	**575754**	**hipk**	**31.7**	**49.6**	**40.65**	**chr3L_575754_hipk**
chr3L	576730	576731	hipk	17.1	15.2	16.15	chr3L_576731_hipk
chr3L	577020	577021	hipk	20	16.9	18.45	chr3L_577021_hipk
chr3L	**577417**	**577418**	**hipk**	**51.42**	**62.12**	**56.77**	**chr3L_577418_hipk**
chr3L	577970	577971	hipk	21.4	25.9	23.65	chr3L_577971_hipk
chr3L	578186	578187	hipk	18.2	24.9	21.55	chr3L_578187_hipk
chr3L	578453	578454	hipk	25.7	32.7	29.2	chr3L_578454_hipk
chr3L	579335	579336	hipk	18.1	17	17.55	chr3L_579336_hipk
chr3L	579634	579635	hipk	20.5	19.8	20.15	chr3L_579635_hipk

bioRxiv preprint doi: https://doi.org/10.1101/2022.02.15.480566; this version posted February 17, 2022. The copyright holder for this preprint (which was not certified by peer review) is the author/funder, who has granted bioRxiv a license to display the preprint in perpetuity. It is made available under aCC-BY-NC-ND 4.0 International license.

chr3L	**580103**	**580104**	**hipk**	**63.1**	**67.7**	**65.4**	**chr3L_580104_hipk**
chr3L	580500	580501	hipk	15.6	18.1	16.85	chr3L_580501_hipk
chr3L	580932	580933	hipk	17.9	24.1	21	chr3L_580933_hipk
chr3L	**8970787**	**8970788**	**CG5026**	**17.9**	**16.7**	**17.3**	**chr3L_8970788_CG5026**
chr3L	8993382	8993383	smg	25.9	15.3	20.6	chr3L_8993383_smg
chr3L	9074752	9074753	Tequila	29.8	19.5	24.65	chr3L_9074753_Tequila
chr3L	**9103274**	**9103275**	**bol**	**23.9**	**26.3**	**25.1**	**chr3L_9103275_bol**
chr3L	9136454	9136455	Use1	25	16	20.5	chr3L_9136455_Use1
chr3L	9669496	9669497	fry	18.2	18.2	18.2	chr3L_9669497_fry
chr3L	9945905	9945906	CG34356	19.4	32.1	25.75	chr3L_9945906_CG34356
chr3R	10158991	10158992	Invadolysin	17.9	18.2	18.05	chr3R_10158992_Invadolysin
chr3R	10862820	10862821	CG6574	20.8	33.3	27.05	chr3R_10862821_CG6574
chr3R	10877257	10877258	CR45195	32.7	19.5	26.1	chr3R_10877258_CR45195
chr3R	10889941	10889942	Leash	18.2	18.8	18.5	chr3R_10889942_Leash
chr3R	**13224637**	**13224638**	**Ace**	**24.8**	**33.3**	**29.05**	**chr3R_13224638_Ace**
chr3R	**13227870**	**13227871**	**Ace**	**26.6**	**35.3**	**30.95**	**chr3R_13227871_Ace**
chr3R	**13227970**	**13227971**	**Ace**	**33.42**	**47.95**	**40.69**	**chr3R_13227971_Ace**
chr3R	14330745	14330746	NK7.1	16.2	16.7	16.45	chr3R_14330746_NK7.1
chr3R	14660839	14660840	Hexim	17.1	20	18.55	chr3R_14660840_Hexim
chr3R	14669984	14669985	Meltrin	16.95	20.7	18.82	chr3R_14669985_Meltrin
chr3R	14746335	14746336	jvl	36.4	20.9	28.65	chr3R_14746336_jvl
chr3R	14746546	14746547	smp-30	45.1	24	34.55	chr3R_14746547_smp-30
chr3R	**14804349**	**14804350**	**btsz**	**16.5**	**26.5**	**21.5**	**chr3R_14804350_btsz**
chr3R	**15255687**	**15255688**	**CG42404**	**18.2**	**17.6**	**17.9**	**chr3R_15255688_CG42404**
chr3R	15356475	15356476	Atg4b	15.4	20.7	18.05	chr3R_15356476_Atg4b
chr3R	15414730	15414731	Atx2	22.82	26.25	24.54	chr3R_15414731_Atx2
chr3R	15414731	15414732	Atx2	19	22.6	20.8	chr3R_15414732_Atx2
chr3R	15849417	15849418	cv-d	18.8	22.2	20.5	chr3R_15849418_cv-d
chr3R	**16611267**	**16611268**	**NPF**	**22.98**	**23.52**	**23.25**	**chr3R_16611268_NPF**
chr3R	16645743	16645744	CG10324	26.1	35	30.55	chr3R_16645744_CG10324
chr3R	17090737	17090738	cal1	25	15.4	20.2	chr3R_17090738_cal1
chr3R	**17731884**	**17731885**	**Lgr1**	**20**	**19**	**19.5**	**chr3R_17731885_Lgr1**
chr3R	17802763	17802764	CG17806	20.7	18.8	19.75	chr3R_17802764_CG17806
chr3R	19155252	19155253	CG11779	15.6	19.1	17.35	chr3R_19155253_CG11779
chr3R	20783186	20783187	Syp	21.1	17	19.05	chr3R_20783187_Syp
chr3R	20797469	20797470	Syp	15.3	20	17.65	chr3R_20797470_Syp
chr3R	20820785	20820786	CG17271	31.2	19.75	25.48	chr3R_20820786_CG17271
chr3R	20862212	20862213	CG3822	17	26.3	21.65	chr3R_20862213_CG3822
chr3R	20992668	20992669	Calx	17.8	27.5	22.65	chr3R_20992669_Calx
chr3R	21213891	21213892	SNF4Agamma	17.2	20	18.6	chr3R_21213892_SNF4Agamma
chr3R	21354284	21354285	mod(mdg4)	15	19	17	chr3R_21354285_mod(mdg4)
chr3R	21527750	21527751	CG7956	30.3	26.5	28.4	chr3R_21527751_CG7956
chr3R	21625731	21625732	E2f	18	23.7	20.85	chr3R_21625732_E2f
chr3R	23261698	23261699	orb	15.2	16.1	15.65	chr3R_23261699_orb

bioRxiv preprint doi: https://doi.org/10.1101/2022.02.15.480566; this version posted February 17, 2022. The copyright holder for this preprint (which was not certified by peer review) is the author/funder, who has granted bioRxiv a license to display the preprint in perpetuity. It is made available under aCC-BY-NC-ND 4.0 International license.

chr3R	23681818	23681819	eIF-3p66	20.4	21.5	20.95	chr3R_23681819_eIF-3p66
chr3R	**23698883**	**23698884**	**prt**	**15.4**	**23.4**	**19.4**	**chr3R_23698884_prt**
chr3R	23723418	23723419	CG10365	16.1	21.1	18.6	chr3R_23723419_CG10365
chr3R	23732353	23732354	Rpn9	20.4	16.7	18.55	chr3R_23732354_Rpn9
chr3R	24664388	24664389	slo	23.1	30	26.55	chr3R_24664389_slo
chr3R	24802164	24802165	polybromo	29.2	20.98	25.09	chr3R_24802165_polybromo
chr3R	24820485	24820486	Saf-B	15	22	18.5	chr3R_24820486_Saf-B
chr3R	25234647	25234648	CG10420	22.2	34.5	28.35	chr3R_25234648_CG10420
chr3R	**26233920**	**26233921**	**CG12290**	**25.6**	**18.4**	**22**	**chr3R_26233921_CG12290**
chr3R	**28050111**	**28050112**	**CG34362**	**15.6**	**25.6**	**20.6**	**chr3R_28050112_CG34362**
chr3R	28838531	28838532	Apc	20.4	18.8	19.6	chr3R_28838532_Apc
chr3R	29659085	29659086	Dop1R2	15.8	39.5	27.65	chr3R_29659086_Dop1R2
chr3R	**29674515**	**29674516**	**Bub3**	**27.6**	**17.8**	**22.7**	**chr3R_29674516_Bub3**
chr3R	31457698	31457699	Gprk2	23.5	24.5	24	chr3R_31457699_Gprk2
chr3R	31841367	31841368	RhoGAP100F	17.73	19	18.37	chr3R_31841368_RhoGAP100F
chr3R	**5811503**	**5811504**	**CG11000**	**21.3**	**32.4**	**26.85**	**chr3R_5811504_CG11000**
chr3R	**5811505**	**5811506**	**CG11000**	**20.8**	**25.7**	**23.25**	**chr3R_5811506_CG11000**
chr3R	7126383	7126384	CG10098	18.6	19.1	18.85	chr3R_7126384_CG10098
chr3R	8244435	8244436	CG18749	15.4	16.1	15.75	chr3R_8244436_CG18749
chr3R	8244435	8244436	CG33722	15.4	16.1	15.75	chr3R_8244436_CG33722
chr3R	9416762	9416763	alpha-Man-II	30.8	32.3	31.55	chr3R_9416763_alpha-Man-II
chr3R	9441505	9441506	ps	37.92	33.52	35.72	chr3R_9441506_ps
chr3R	9471135	9471136	CG16779	43.05	34.85	38.95	chr3R_9471136_CG16779
chr3R	9525979	9525980	CG8176	16.2	24.4	20.3	chr3R_9525980_CG8176
chr3R	9539464	9539465	mura	21.75	20.05	20.9	chr3R_9539465_mura
chr3R	9794186	9794187	CG8516	19.4	30.8	25.1	chr3R_9794187_CG8516
chr4	478956	478957	Asator	15.1	20	17.55	chr4_478957_Asator
chr4	532906	532907	zfh2	20	19.7	19.85	chr4_532907_zfh2
chr4	92946	92947	pan	22.5	20.8	21.65	chr4_92947_pan
chrX	10309093	10309094	alpha-Man-I	24.5	29	26.75	chrX_10309094_alpha-Man-I
chrX	**12331302**	**12331303**	**Ten-a**	**34.8**	**34**	**34.4**	**chrX_12331303_Ten-a**
chrX	16075472	16075473	Tob	23.68	29.32	26.5	chrX_16075473_Tob
chrX	16075887	16075888	Tob	22.2	22	22.1	chrX_16075888_Tob
chrX	16075888	16075889	Tob	21.6	24	22.8	chrX_16075889_Tob
chrX	**16076959**	**16076960**	**Tob**	**20**	**23.3**	**21.65**	**chrX_16076960_Tob**
chrX	16077193	16077194	Tob	17.85	19.15	18.5	chrX_16077194_Tob
chrX	16089317	16089318	Tob	15.2	16.1	15.65	chrX_16089318_Tob
chrX	**3321068**	**3321069**	**dnc**	**22.7**	**28.9**	**25.8**	**chrX_3321069_dnc**
chrX	**3342369**	**3342370**	**dnc**	**17.4**	**22.2**	**19.8**	**chrX_3342370_dnc**
chrX	**6325433**	**6325434**	**CG15894**	**32**	**20.8**	**26.4**	**chrX_6325434_CG15894**
chrX	**9172798**	**9172799**	**mei-P26**	**17.3**	**23.1**	**20.2**	**chrX_9172799_mei-P26**
chrX	9179452	9179453	mei-P26	17.35	22.23	19.79	chrX_9179453_mei-P26
chrX	9188891	9188892	mei-P26	15.8	18.4	17.1	chrX_9188892_mei-P26

774
775

bioRxiv preprint doi: https://doi.org/10.1101/2022.02.15.480566; this version posted February 17, 2022. The copyright holder for this preprint (which was not certified by peer review) is the author/funder, who has granted bioRxiv a license to display the preprint in perpetuity. It is made available under aCC-BY-NC-ND 4.0 International license.

776 **BIBLIOGRAPHY:**

777
778 Alberti S, Gladfelter A, Mittag T (2019) Considerations and Challenges in Studying Liquid-
779 Liquid Phase Separation and Biomolecular Condensates. *Cell* 176: 419-434
780
781 Alberti S, Mateju D, Mediani L, Carra S (2017) Granulostasis: Protein Quality Control of RNP
782 Granules. *Frontiers in Molecular Neuroscience* 10
783
784 Andrusiak MG, Sharifnia P, Lyu X, Wang Z, Dickey AM, Wu Z, Chisholm AD, Jin Y (2019)
785 Inhibition of Axon Regeneration by Liquid-like TIAR-2 Granules. *Neuron* 104: 290-304.e298
786
787 Ash PEA, Lei S, Shattuck J, Boudeau S, Carlomagno Y, Medalla M, Mashimo BL, Socorro G,
788 Al-Mohanna LFA, Jiang L *et al* (2021) TIA1 potentiates tau phase separation and promotes
789 generation of toxic oligomeric tau. *Proceedings of the National Academy of Sciences* 118:
790 e2014188118
791
792 Azkanaz M, Rodríguez López A, De Boer B, Huiting W, Angrand P-O, Vellenga E, Kampinga
793 HH, Bergink S, Martens JH, Schuringa JJ *et al* (2019) Protein quality control in the nucleolus
794 safeguards recovery of epigenetic regulators after heat shock. *eLife* 8
795
796 Babinchak WM, Surewicz WK (2020) Liquid–Liquid Phase Separation and Its Mechanistic
797 Role in Pathological Protein Aggregation. *Journal of Molecular Biology* 432: 1910-1925
798
799 Bah A, Forman-Kay JD (2016) Modulation of Intrinsically Disordered Protein Function by
800 Post-translational Modifications. *Journal of Biological Chemistry* 291: 6696-6705
801
802 Bah A, Vernon RM, Siddiqui Z, Krzeminski M, Muhandiram R, Zhao C, Sonenberg N, Kay
803 LE, Forman-Kay JD (2015) Folding of an intrinsically disordered protein by phosphorylation
804 as a regulatory switch. *Nature* 519: 106-109
805
806 Bakthavachalu B, Huelsmeier J, Sudhakaran IP, Hillebrand J, Singh A, Petrauskas A,
807 Thiagarajan D, Sankaranarayanan M, Mizoue L, Anderson EN *et al* (2018) RNP-Granule
808 Assembly via Ataxin-2 Disordered Domains Is Required for Long-Term Memory and
809 Neurodegeneration. *Neuron* 98: 754-766.e754
810
811 Becker LA, Huang B, Bieri G, Ma R, Knowles DA, Jafar-Nejad P, Messing J, Kim HJ, Soriano
812 A, Auburger G *et al* (2017) Therapeutic reduction of ataxin-2 extends lifespan and reduces
813 pathology in TDP-43 mice. *Nature* 544: 367-371
814
815 Berlow RB, Dyson HJ, Wright PE (2015) Functional advantages of dynamic protein disorder.
816 *FEBS Lett* 589: 2433-2440
817
818 Bevilacqua PC, Williams AM, Chou H-L, Assmann SM (2022) RNA multimerization as an
819 organizing force for liquid–liquid phase separation. *RNA* 28: 16-26
820
821 Biogen, 2021. https://clinicaltrials.gov/ct2/show/NCT04494256.
822
823 Boeynaems S, Dorone Y, Marian A, Shabardina V, Huang G, Kim G, Sanyal A, Şen N-E,
824 Docampo R, Ruiz-Trillo I *et al* (2021) Poly(A)-binding protein is an ataxin-2 chaperone that
825 emulsifies biomolecular condensates. *bioRxiv*: 2021.2008.2023.457426

bioRxiv preprint doi: https://doi.org/10.1101/2022.02.15.480566; this version posted February 17, 2022. The copyright holder for this preprint (which was not certified by peer review) is the author/funder, who has granted bioRxiv a license to display the preprint in perpetuity. It is made available under aCC-BY-NC-ND 4.0 International license.

826
827 Brandmann T, Fakim H, Padamsi Z, Youn JY, Gingras AC, Fabian MR, Jinek M (2018)
828 Molecular architecture of LSM14 interactions involved in the assembly of mRNA silencing
829 complexes. *Embo j* 37
830
831 Buchan JR (2014) mRNP granules. *RNA Biology* 11: 1019-1030
832
833 Calabretta S, Richard S (2015) Emerging Roles of Disordered Sequences in RNA-Binding
834 Proteins. *Trends Biochem Sci* 40: 662-672
835
836 Cao X, Jin X, Liu B (2020) The involvement of stress granules in aging and aging-associated
837 diseases. *Aging Cell* 19
838
839 Chou A, Krukowski K, Jopson T, Zhu PJ, Costa-Mattioli M, Walter P, Rosi S (2017) Inhibition
840 of the integrated stress response reverses cognitive deficits after traumatic brain injury. *Proc*
841 *Natl Acad Sci U S A* 114: E6420-e6426
842
843 Cirulli ET, Lasseigne BN, Petrovski S, Sapp PC, Dion PA, Leblond CS, Couthouis J, Lu YF,
844 Wang Q, Krueger BJ *et al* (2015) Exome sequencing in amyotrophic lateral sclerosis identifies
845 risk genes and pathways. *Science* 347: 1436-1441
846
847 Couthouis J, Hart MP, Erion R, King OD, Diaz Z, Nakaya T, Ibrahim F, Kim H-J, Mojsilovic-
848 Petrovic J, Panossian S *et al* (2012) Evaluating the role of the FUS/TLS-related gene EWSR1
849 in amyotrophic lateral sclerosis. *Human Molecular Genetics* 21: 2899-2911
850
851 Damrath E, Heck MV, Gispert S, Azizov M, Nowock J, Seifried C, Rüb U, Walter M, Auburger
852 G (2012) ATXN2-CAG42 Sequesters PABPC1 into Insolubility and Induces FBXW8 in
853 Cerebellum of Old Ataxic Knock-In Mice. *PLoS Genetics* 8: e1002920
854
855 De Graeve F, Besse F (2018) Neuronal RNP granules: from physiological to pathological
856 assemblies. *Biological Chemistry* 399: 623-635
857
858 Decker CJ, Teixeira D, Parker R (2007) Edc3p and a glutamine/asparagine-rich domain of
859 Lsm4p function in processing body assembly in Saccharomyces cerevisiae. *J Cell Biol* 179:
860 437-449
861
862 Deo RC, Bonanno JB, Sonenberg N, Burley SK (1999) Recognition of Polyadenylate RNA by
863 the Poly(A)-Binding Protein. *Cell* 98: 835-845
864
865 Elden AC, Kim HJ, Hart MP, Chen-Plotkin AS, Johnson BS, Fang X, Armakola M, Geser F,
866 Greene R, Lu MM *et al* (2010) Ataxin-2 intermediate-length polyglutamine expansions are
867 associated with increased risk for ALS. *Nature* 466: 1069-1075
868
869 Formicola N, Vijayakumar J, Besse F (2019) Neuronal ribonucleoprotein granules: Dynamic
870 sensors of localized signals. *Traffic* 20: 639-649
871
872 Gilks N, Kedersha N, Ayodele M, Shen L, Stoecklin G, Dember LM, Anderson P (2004) Stress
873 granule assembly is mediated by prion-like aggregation of TIA-1. *Mol Biol Cell* 15: 5383-5398

bioRxiv preprint doi: https://doi.org/10.1101/2022.02.15.480566; this version posted February 17, 2022. The copyright holder for this preprint (which was not certified by peer review) is the author/funder, who has granted bioRxiv a license to display the preprint in perpetuity. It is made available under aCC-BY-NC-ND 4.0 International license.

874 Ginsberg SD, Galvin JE, Chiu TS, Lee VM, Masliah E, Trojanowski JQ (1998) RNA
875 sequestration to pathological lesions of neurodegenerative diseases. *Acta Neuropathol* 96: 487-
876 494
877
878 Gomes E, Shorter J (2019) The molecular language of membraneless organelles. *J Biol Chem*
879 294: 7115-7127
880
881 Hachet O, Ephrussi A (2004) Splicing of oskar RNA in the nucleus is coupled to its cytoplasmic
882 localization. *Nature* 428: 959-963
883
884 Halliday M, Radford H, Zents KAM, Molloy C, Moreno JA, Verity NC, Smith E, Ortori CA,
885 Barrett DA, Bushell M *et al* (2017) Repurposed drugs targeting eIF2α-P-mediated translational
886 repression prevent neurodegeneration in mice. *Brain* 140: 1768-1783
887
888 Han TW, Kato M, Xie S, Wu LC, Mirzaei H, Pei J, Chen M, Xie Y, Allen J, Xiao G *et al*
889 (2012) Cell-free formation of RNA granules: bound RNAs identify features and components
890 of cellular assemblies. *Cell* 149: 768-779
891
892 Harlen KM, Churchman LS (2017) The code and beyond: transcription regulation by the RNA
893 polymerase II carboxy-terminal domain. *Nature Reviews Molecular Cell Biology* 18: 263-273
894
895 Hetz C, Zhang K, Kaufman RJ (2020) Mechanisms, regulation and functions of the unfolded
896 protein response. *Nature Reviews Molecular Cell Biology* 21: 421-438
897
898 Hochberg-Laufer H, Schwed-Gross A, Neugebauer KM, Shav-Tal Y (2019) Uncoupling of
899 nucleo-cytoplasmic RNA export and localization during stress. *Nucleic Acids Research* 47:
900 4778-4797
901
902 Hofweber M, Dormann D (2019) Friend or foe—Post-translational modifications as regulators
903 of phase separation and RNP granule dynamics. *Journal of Biological Chemistry* 294: 7137-
904 7150
905
906 Huelsmeier J, Walker E, Bakthavachalu B, Ramaswami M (2021) A C-terminal ataxin-2
907 disordered region promotes Huntingtin protein aggregation and neurodegeneration in
908 Drosophila models of Huntington's disease. *G3 (Bethesda)* 11
909
910 Hyman AA, Weber CA, Jülicher F (2014) Liquid-Liquid Phase Separation in Biology. *Annual*
911 *Review of Cell and Developmental Biology* 30: 39-58
912
913 Inagaki H, Hosoda N, Tsuiji H, Hoshino S-I (2020) Direct evidence that Ataxin-2 is a
914 translational activator mediating cytoplasmic polyadenylation. *Journal of Biological*
915 *Chemistry* 295: 15810-15825
916
917 Ivanov P, Kedersha N, Anderson P (2019) Stress Granules and Processing Bodies in
918 Translational Control. *Cold Spring Harb Perspect Biol* 11
919
920 Jain A, Vale RD (2017) RNA phase transitions in repeat expansion disorders. *Nature* 546: 243-
921 247
922

bioRxiv preprint doi: https://doi.org/10.1101/2022.02.15.480566; this version posted February 17, 2022. The copyright holder for this preprint (which was not certified by peer review) is the author/funder, who has granted bioRxiv a license to display the preprint in perpetuity. It is made available under aCC-BY-NC-ND 4.0 International license.

923 Järvelin AI, Noerenberg M, Davis I, Castello A (2016) The new (dis)order in RNA regulation.
924 *Cell Commun Signal* 14: 9
925
926 Jiang S, Fagman JB, Chen C, Alberti S, Liu B (2020) Protein phase separation and its role in
927 tumorigenesis. *eLife* 9
928
929 Jiménez-López D, Guzmán P (2014) Insights into the evolution and domain structure of ataxin-
930 2 proteins across eukaryotes. *BMC Research Notes* 7: 453
931
932 Kaehler C, Isensee J, Nonhoff U, Terrey M, Hucho T, Lehrach H, Krobitsch S (2012) Ataxin-
933 2-like is a regulator of stress granules and processing bodies. *PLoS One* 7: e50134
934
935 Kato M, Han TW, Xie S, Shi K, Du X, Wu LC, Mirzaei H, Goldsmith EJ, Longgood J, Pei J
936 *et al* (2012) Cell-free formation of RNA granules: low complexity sequence domains form
937 dynamic fibers within hydrogels. *Cell* 149: 753-767
938
939 Kedersha N, Anderson P (2007) Mammalian stress granules and processing bodies. *Methods*
940 *Enzymol* 431: 61-81
941
942 Kedersha N, Panas MD, Achorn CA, Lyons S, Tisdale S, Hickman T, Thomas M, Lieberman
943 J, McInerney GM, Ivanov P *et al* (2016) G3BP-Caprin1-USP10 complexes mediate stress
944 granule condensation and associate with 40S subunits. *J Cell Biol* 212: 845-860
945
946 Kedersha NL, Gupta M, Li W, Miller I, Anderson P (1999) RNA-Binding Proteins Tia-1 and
947 Tiar Link the Phosphorylation of Eif-2α to the Assembly of Mammalian Stress Granules.
948 *Journal of Cell Biology* 147: 1431-1442
949
950 Khong A, Parker R (2020) The landscape of eukaryotic mRNPs. *RNA* 26: 229-239
951
952 Kiebler MA, Bassell GJ (2006) Neuronal RNA granules: movers and makers. *Neuron* 51: 685-
953 690
954
955 Kim G, Gautier O, Tassoni-Tsuchida E, Ma XR, Gitler AD (2020) ALS Genetics: Gains,
956 Losses, and Implications for Future Therapies. *Neuron* 108: 822-842
957
958 Kim H-J, Raphael AR, Ladow ES, Mcgurk L, Weber RA, Trojanowski JQ, Lee VM-Y,
959 Finkbeiner S, Gitler AD, Bonini NM (2014) Therapeutic modulation of eIF2α phosphorylation
960 rescues TDP-43 toxicity in amyotrophic lateral sclerosis disease models. *Nature Genetics* 46:
961 152-160
962
963 Kim HJ, Kim NC, Wang YD, Scarborough EA, Moore J, Diaz Z, MacLea KS, Freibaum B, Li
964 S, Molliex A *et al* (2013) Mutations in prion-like domains in hnRNPA2B1 and hnRNPA1
965 cause multisystem proteinopathy and ALS. *Nature* 495: 467-473
966
967 Kim TH, Payliss BJ, Nosella ML, Lee ITW, Toyama Y, Forman-Kay JD, Kay LE (2021)
968 Interaction hot spots for phase separation revealed by NMR studies of a CAPRIN1 condensed
969 phase. *Proc Natl Acad Sci U S A* 118
970
971 Knowles RB, Sabry JH, Martone ME, Deerinck TJ, Ellisman MH, Bassell GJ, Kosik KS (1996)
972 Translocation of RNA Granules in Living Neurons. *The Journal of Neuroscience* 16: 7812

bioRxiv preprint doi: https://doi.org/10.1101/2022.02.15.480566; this version posted February 17, 2022. The copyright holder for this preprint (which was not certified by peer review) is the author/funder, who has granted bioRxiv a license to display the preprint in perpetuity. It is made available under aCC-BY-NC-ND 4.0 International license.

973
974 Kozlov G, Safaee N, Rosenauer A, Gehring K (2010) Structural basis of binding of P-body-
975 associated proteins GW182 and ataxin-2 by the Mlle domain of poly(A)-binding protein. *J Biol*
976 *Chem* 285: 13599-13606
977
978 Kwon I, Kato M, Xiang S, Wu L, Theodoropoulos P, Mirzaei H, Han T, Xie S, Corden Jeffry L,
979 McKnight Steven L (2013) Phosphorylation-Regulated Binding of RNA Polymerase II to
980 Fibrous Polymers of Low-Complexity Domains. *Cell* 155: 1049-1060
981
982 Latonen L (2019) Phase-to-Phase With Nucleoli – Stress Responses, Protein Aggregation and
983 Novel Roles of RNA. *Frontiers in Cellular Neuroscience* 13: 151
984
985 Lee J, Yoo E, Lee H, Park K, Hur JH, Lim C (2017) LSM12 and ME31B/DDX6 Define
986 Distinct Modes of Posttranscriptional Regulation by ATAXIN-2 Protein Complex in
987 Drosophila Circadian Pacemaker Neurons. *Mol Cell* 66: 129-140.e127
988
989 Lee KH, Zhang P, Kim HJ, Mitrea DM, Sarkar M, Freibaum BD, Cika J, Coughlin M, Messing
990 J, Molliex A *et al* (2016) C9orf72 Dipeptide Repeats Impair the Assembly, Dynamics, and
991 Function of Membrane-Less Organelles. *Cell* 167: 774-788.e717
992
993 Li YR, King OD, Shorter J, Gitler AD (2013) Stress granules as crucibles of ALS pathogenesis.
994 *J Cell Biol* 201: 361-372
995
996 Lim C, Allada R (2013) ATAXIN-2 activates PERIOD translation to sustain circadian rhythms
997 in Drosophila. *Science* 340: 875-879
998
999 Lin Y, Currie SL, Rosen MK (2017) Intrinsically disordered sequences enable modulation of
1000 protein phase separation through distributed tyrosine motifs. *J Biol Chem* 292: 19110-19120
1001
1002 Lin Y, Protter SW, David, Rosen K, Michael, Parker R (2015) Formation and Maturation of
1003 Phase-Separated Liquid Droplets by RNA-Binding Proteins. *Molecular Cell* 60: 208-219
1004
1005 Liu EY, Cali CP, Lee EB (2017) RNA metabolism in neurodegenerative disease. *Dis Model*
1006 *Mech* 10: 509-518
1007
1008 Machida K, Shigeta T, Yamamoto Y, Ito T, Svitkin Y, Sonenberg N, Imataka H (2018)
1009 Dynamic interaction of poly(A)-binding protein with the ribosome. *Scientific Reports* 8: 17435
1010 Mallucci GR, Klenerman D, Rubinsztein DC (2020) Developing Therapies for
1011 Neurodegenerative Disorders: Insights from Protein Aggregation and Cellular Stress
1012 Responses. *Annual Review of Cell and Developmental Biology* 36: 165-189
1013
1014 Mandrioli J, Mediani L, Alberti S, Carra S (2020) ALS and FTD: Where RNA metabolism
1015 meets protein quality control. *Semin Cell Dev Biol* 99: 183-192
1016
1017 Mangus DA, Evans MC, Jacobson A (2003) Poly(A)-binding proteins: multifunctional
1018 scaffolds for the post-transcriptional control of gene expression. *Genome Biol* 4: 223
1019
1020 Maniatis T, Reed R (2002) An extensive network of coupling among gene expression
1021 machines. *Nature* 416: 499-506
1022

bioRxiv preprint doi: https://doi.org/10.1101/2022.02.15.480566; this version posted February 17, 2022. The copyright holder for this preprint (which was not certified by peer review) is the author/funder, who has granted bioRxiv a license to display the preprint in perpetuity. It is made available under aCC-BY-NC-ND 4.0 International license.

1023 Martin KC, Ephrussi A (2009) mRNA localization: gene expression in the spatial dimension.
1024 *Cell* 136: 719-730
1025
1026 Matheny T, Van Treeck B, Huynh TN, Parker R (2021) RNA partitioning into stress granules
1027 is based on the summation of multiple interactions. *RNA* 27: 174-189
1028
1029 McCann C, Holohan EE, Das S, Dervan A, Larkin A, Lee JA, Rodrigues V, Parker R,
1030 Ramaswami M (2011) The Ataxin-2 protein is required for microRNA function and synapse-
1031 specific long-term olfactory habituation. *Proc Natl Acad Sci U S A* 108: E655-662
1032
1033 McMahon AC, Rahman R, Jin H, Shen JL, Fieldsend A, Luo W, Rosbash M (2016) TRIBE:
1034 Hijacking an RNA-Editing Enzyme to Identify Cell-Specific Targets of RNA-Binding
1035 Proteins. *Cell* 165: 742-753
1036
1037 Murray DT, Kato M, Lin Y, Thurber KR, Hung I, McKnight SL, Tycko R (2017) Structure of
1038 FUS Protein Fibrils and Its Relevance to Self-Assembly and Phase Separation of Low-
1039 Complexity Domains. *Cell* 171: 615-627.e616
1040
1041 Murthy AC, Dignon GL, Kan Y, Zerze GH, Parekh SH, Mittal J, Fawzi NL (2019) Molecular
1042 interactions underlying liquid−liquid phase separation of the FUS low-complexity domain.
1043 *Nature Structural & Molecular Biology* 26: 637-648
1044
1045 Nonhoff U, Ralser M, Welzel F, Piccini I, Balzereit D, Yaspo ML, Lehrach H, Krobitsch S
1046 (2007) Ataxin-2 interacts with the DEAD/H-box RNA helicase DDX6 and interferes with P-
1047 bodies and stress granules. *Mol Biol Cell* 18: 1385-1396
1048
1049 Patel A, Lee HO, Jawerth L, Maharana S, Jahnel M, Hein MY, Stoynov S, Mahamid J, Saha
1050 S, Franzmann TM *et al* (2015) A Liquid-to-Solid Phase Transition of the ALS Protein FUS
1051 Accelerated by Disease Mutation. *Cell* 162: 1066-1077
1052
1053 Preissler S, Ron D (2019) Early Events in the Endoplasmic Reticulum Unfolded Protein
1054 Response. *Cold Spring Harb Perspect Biol* 11
1055
1056 Protter DSW, Parker R (2016) Principles and Properties of Stress Granules. *Trends Cell Biol*
1057 26: 668-679
1058
1059 Protter DSW, Rao BS, Van Treeck B, Lin Y, Mizoue L, Rosen MK, Parker R (2018)
1060 Intrinsically Disordered Regions Can Contribute Promiscuous Interactions to RNP Granule
1061 Assembly. *Cell Rep* 22: 1401-1412
1062
1063 Ramaswami M, Taylor JP, Parker R (2013) Altered ribostasis: RNA-protein granules in
1064 degenerative disorders. *Cell* 154: 727-736
1065
1066 Rayman JB, Karl KA, Kandel ER (2018) TIA-1 Self-Multimerization, Phase Separation, and
1067 Recruitment into Stress Granules Are Dynamically Regulated by Zn2+. *Cell Reports* 22: 59-
1068 71
1069
1070 Saito M, Hess D, Eglinger J, Fritsch AW, Kreysing M, Weinert BT, Choudhary C, Matthias P
1071 (2019) Acetylation of intrinsically disordered regions regulates phase separation. *Nat Chem*
1072 *Biol* 15: 51-61

bioRxiv preprint doi: https://doi.org/10.1101/2022.02.15.480566; this version posted February 17, 2022. The copyright holder for this preprint (which was not certified by peer review) is the author/funder, who has granted bioRxiv a license to display the preprint in perpetuity. It is made available under aCC-BY-NC-ND 4.0 International license.

1073
1074 Satterfield TF, Pallanck LJ (2006) Ataxin-2 and its Drosophila homolog, ATX2, physically
1075 assemble with polyribosomes. *Hum Mol Genet* 15: 2523-2532
1076
1077 Schuller AP, Wojtynek M, Mankus D, Tatli M, Kronenberg-Tenga R, Regmi SG, Dip PV,
1078 Lytton-Jean AKR, Brignole EJ, Dasso M *et al* (2021) The cellular environment shapes the
1079 nuclear pore complex architecture. *Nature* 598: 667-671
1080
1081 Scoles DR, Meera P, Schneider MD, Paul S, Dansithong W, Figueroa KP, Hung G, Rigo F,
1082 Bennett CF, Otis TS *et al* (2017) Antisense oligonucleotide therapy for spinocerebellar ataxia
1083 type 2. *Nature* 544: 362-366
1084
1085 Shin Y, Brangwynne CP (2017) Liquid phase condensation in cell physiology and disease.
1086 *Science* 357
1087
1088 Shulman JM, Feany MB (2003) Genetic Modifiers of Tauopathy in Drosophila. *Genetics* 165:
1089 1233-1242
1090
1091 Sidrauski C, Mcgeachy AM, Ingolia NT, Walter P (2015) The small molecule ISRIB reverses
1092 the effects of eIF2α phosphorylation on translation and stress granule assembly. *eLife* 4
1093
1094 Singh A, Hulsmeier J, Kandi AR, Pothapragada SS, Hillebrand J, Petrauskas A, Agrawal K,
1095 Rt K, Thiagarajan D, Jayaprakashappa D *et al* (2021) Antagonistic roles for Ataxin-2 structured
1096 and disordered domains in RNP condensation. *eLife* 10
1097
1098 Strome S, Wood WB (1982) Immunofluorescence visualization of germ-line-specific
1099 cytoplasmic granules in embryos, larvae, and adults of Caenorhabditis elegans. *Proc Natl Acad*
1100 *Sci U S A* 79: 1558-1562
1101
1102 Sudhakaran IP, Hillebrand J, Dervan A, Das S, Holohan EE, Hülsmeier J, Sarov M, Parker R,
1103 VijayRaghavan K, Ramaswami M (2014) FMRP and Ataxin-2 function together in long-term
1104 olfactory habituation and neuronal translational control. *Proc Natl Acad Sci U S A* 111: E99-
1105 E108
1106
1107 Taylor JP, Brown RH, Cleveland DW (2016) Decoding ALS: from genes to mechanism.
1108 *Nature* 539: 197-206
1109
1110 Tillotson R, Selfridge J, Koerner MV, Gadalla KKE, Guy J, De Sousa D, Hector RD, Cobb
1111 SR, Bird A (2017) Radically truncated MeCP2 rescues Rett syndrome-like neurological
1112 defects. *Nature* 550: 398-401
1113
1114 Toretsky JA, Wright PE (2014) Assemblages: functional units formed by cellular phase
1115 separation. *J Cell Biol* 206: 579-588
1116
1117 Trapnell C, Pachter L, Salzberg SL (2009) TopHat: discovering splice junctions with RNA-
1118 Seq. *Bioinformatics* 25: 1105-1111
1119
1120 Van Treeck B, Parker R (2018) Emerging Roles for Intermolecular RNA-RNA Interactions in
1121 RNP Assemblies. *Cell* 174: 791-802
1122

bioRxiv preprint doi: https://doi.org/10.1101/2022.02.15.480566; this version posted February 17, 2022. The copyright holder for this preprint (which was not certified by peer review) is the author/funder, who has granted bioRxiv a license to display the preprint in perpetuity. It is made available under aCC-BY-NC-ND 4.0 International license.

1123 Van Treeck B, Protter DSW, Matheny T, Khong A, Link CD, Parker R (2018) RNA self-
1124 assembly contributes to stress granule formation and defining the stress granule transcriptome.
1125 *Proc Natl Acad Sci U S A* 115: 2734-2739
1126
1127 Vogler TO, Wheeler JR, Nguyen ED, Hughes MP, Britson KA, Lester E, Rao B, Betta ND,
1128 Whitney ON, Ewachiw TE *et al* (2018) TDP-43 and RNA form amyloid-like myo-granules in
1129 regenerating muscle. *Nature* 563: 508-513
1130
1131 Wang F, Li J, Fan S, Jin Z, Huang C (2020) Targeting stress granules: A novel therapeutic
1132 strategy for human diseases. *Pharmacological Research* 161: 105143
1133
1134 Wheeler JR, Matheny T, Jain S, Abrisch R, Parker R (2016) Distinct stages in stress granule
1135 assembly and disassembly. *eLife* 5
1136
1137 Wolozin B, Ivanov P (2019) Stress granules and neurodegeneration. *Nature Reviews*
1138 *Neuroscience* 20: 649-666
1139
1140 Wong YL, Lebon L, Edalji R, Lim HB, Sun C, Sidrauski C (2018) The small molecule ISRIB
1141 rescues the stability and activity of Vanishing White Matter Disease eIF2B mutant complexes.
1142 *eLife* 7
1143
1144 Xie J, Kozlov G, Gehring K (2014) The "tale" of poly(A) binding protein: the MLLE domain
1145 and PAM2-containing proteins. *Biochim Biophys Acta* 1839: 1062-1068
1146
1147 Yang P, Mathieu C, Kolaitis RM, Zhang P, Messing J, Yurtsever U, Yang Z, Wu J, Li Y, Pan
1148 Q *et al* (2020) G3BP1 Is a Tunable Switch that Triggers Phase Separation to Assemble Stress
1149 Granules. *Cell* 181: 325-345.e328
1150
1151 Yi H, Park J, Ha M, Lim J, Chang H, Kim VN (2018) PABP Cooperates with the CCR4-NOT
1152 Complex to Promote mRNA Deadenylation and Block Precocious Decay. *Mol Cell* 70: 1081-
1153 1088.e1085
1154
1155 Yokoshi M, Li Q, Yamamoto M, Okada H, Suzuki Y, Kawahara Y (2014) Direct binding of
1156 Ataxin-2 to distinct elements in 3' UTRs promotes mRNA stability and protein expression. *Mol*
1157 *Cell* 55: 186-198
1158
1159 Yoshida M, Yoshida K, Kozlov G, Lim NS, De Crescenzo G, Pang Z, Berlanga JJ, Kahvejian
1160 A, Gehring K, Wing SS *et al* (2006) Poly(A) binding protein (PABP) homeostasis is mediated
1161 by the stability of its inhibitor, Paip2. *The EMBO Journal* 25: 1934-1944
1162
1163 Youn JY, Dyakov BJA, Zhang J, Knight JDR, Vernon RM, Forman-Kay JD, Gingras AC
1164 (2019) Properties of Stress Granule and P-Body Proteomes. *Mol Cell* 76: 286-294
1165
1166 Zhang K, Daigle JG, Cunningham KM, Coyne AN, Ruan K, Grima JC, Bowen KE, Wadhwa
1167 H, Yang P, Rigo F *et al* (2018) Stress Granule Assembly Disrupts Nucleocytoplasmic
1168 Transport. *Cell* 173: 958-971.e917
1169
1170 Zhang Y, Ling J, Yuan C, Dubruille R, Emery P (2013) A role for Drosophila ATX2 in
1171 activation of PER translation and circadian behavior. *Science* 340: 879-882
1172

bioRxiv preprint doi: https://doi.org/10.1101/2022.02.15.480566; this version posted February 17, 2022. The copyright holder for this preprint (which was not certified by peer review) is the author/funder, who has granted bioRxiv a license to display the preprint in perpetuity. It is made available under aCC-BY-NC-ND 4.0 International license.

1173 Zyryanova AF, Kashiwagi K, Rato C, Harding HP, Crespillo-Casado A, Perera LA, Sakamoto
1174 A, Nishimoto M, Yonemochi M, Shirouzu M *et al* (2021) ISRIB Blunts the Integrated Stress
1175 Response by Allosterically Antagonising the Inhibitory Effect of Phosphorylated eIF2 on
1176 eIF2B. *Mol Cell* 81: 88-103.e106
1177